UNIVERSIDAD DE INVESTIGACIÓN DE TECNOLOGÍA EXPERIMENTAL YACHAY

School of Biological Sciences and Engineering

TITTLE: "Retinal reader for the early diagnosis of ocular diseases using image analysis"

Trabajo de integración curricular presentado como requisito para la obtención del título de Ingeniero Biomédico

Author:
Herrera Romero Bryan Stalin

Advisor:
PhD. Salum Graciela Marisa

Co-Advisor:
PhD. Chang Tortolero Oscar Guillermo

Urcuquí, December 2020

Urcuquí, 3 de diciembre de 2020

SECRETARÍA GENERAL
(Vicerrectorado Académico/Cancillería)
ESCUELA DE CIENCIAS BIOLÓGICAS E INGENIERÍA
CARRERA DE BIOMEDICINA
ACTA DE DEFENSA No. UITEY-BIO-2020-00044-AD

A los 3 días del mes de diciembre de 2020, a las 09:30 horas, de manera virtual mediante videoconferencia, y ante el Tribunal Calificador, integrado por los docentes:

Presidente Tribunal de Defensa	Mgs. VILLALBA MENESES, GANDHI FERNANDO
Miembro No Tutor	Dr. TELLKAMP TIETZ, MARKUS PATRICIO , Ph.D.
Tutor	Dra. SALUM , GRACIELA MARISA , Ph.D.

El(la) señor(ita) estudiante HERRERA ROMERO, BRYAN STALIN, con cédula de identidad No. 1724426950, de la ESCUELA DE CIENCIAS BIOLÓGICAS E INGENIERÍA, de la Carrera de BIOMEDICINA, aprobada por el Consejo de Educación Superior (CES), mediante Resolución RPC-SO-43-No.496-2014, realiza a través de videoconferencia, la sustentación de su trabajo de titulación denominado: RETINAL READER FOR THE EARLY DIAGNOSIS OF OCULAR DISEASES USING IMAGE ANALYSIS, previa a la obtención del título de INGENIERO/A BIOMÉDICO/A.

El citado trabajo de titulación, fue debidamente aprobado por el(los) docente(s):

Tutor	Dra. SALUM , GRACIELA MARISA , Ph.D.

Y recibió las observaciones de los otros miembros del Tribunal Calificador, las mismas que han sido incorporadas por el(la) estudiante.

Previamente cumplidos los requisitos legales y reglamentarios, el trabajo de titulación fue sustentado por el(la) estudiante y examinado por los miembros del Tribunal Calificador. Escuchada la sustentación del trabajo de titulación a través de videoconferencia, que integró la exposición de el(la) estudiante sobre el contenido de la misma y las preguntas formuladas por los miembros del Tribunal, se califica la sustentación del trabajo de titulación con las siguientes calificaciones:

Tipo	Docente	Calificación
Miembro Tribunal De Defensa	Dr. TELLKAMP TIETZ, MARKUS PATRICIO , Ph.D.	10,0
Tutor	Dra. SALUM , GRACIELA MARISA , Ph.D.	10,0
Presidente Tribunal De Defensa	Mgs. VILLALBA MENESES, GANDHI FERNANDO	10,0

Lo que da un promedio de: 10 (Diez punto Cero), sobre 10 (diez), equivalente a: APROBADO

Para constancia de lo actuado, firman los miembros del Tribunal Calificador, el/la estudiante y el/la secretario ad-hoc.

Certifico que en cumplimiento del Decreto Ejecutivo 1017 de 16 de marzo de 2020, la defensa de trabajo de titulación (o examen de grado modalidad teórico práctica) se realizó vía virtual, por lo que las firmas de los miembros del Tribunal de Defensa de Grado, constan en forma digital.

HERRERA ROMERO, BRYAN STALIN
Estudiante

GANDHI FERNANDO
VILLALBA MENESES

Mgs. VILLALBA MENESES, GANDHI FERNANDO
Presidente Tribunal de Defensa

GRACIELA
MARISA SALUM

Dra. SALUM , GRACIELA MARISA , Ph.D.
Tutor

Dr. TELLKAMP TIETZ, MARKUS PATRICIO , Ph.D.
Miembro No Tutor

ALARCON FELIX, KARLA ESTEFANIA
Secretario Ad-hoc

AUTORÍA

Yo, **BRYAN STALIN HERRERA ROMERO**, con cédula de identidad 1724426950, declaro que las ideas, juicios, valoraciones, interpretaciones, consultas bibliográficas, definiciones y conceptualizaciones expuestas en el presente trabajo; así cómo, los procedimientos y herramientas utilizadas en la investigación, son de absoluta responsabilidad de el/la autora (a) del trabajo de integración curricular. Así mismo, me acojo a los reglamentos internos de la Universidad de Investigación de Tecnología Experimental Yachay.

Urcuquí, diciembre del 2020.

Bryan Stalin Herrera Romero
CI: 1724426950

AUTORIZACIÓN DE PUBLICACIÓN

Yo, **BRYAN STALIN HERRERA ROMERO,** con cédula de identidad 1724426950, cedo a la Universidad de Tecnología Experimental Yachay, los derechos de publicación de la presente obra, sin que deba haber un reconocimiento económico por este concepto. Declaro además que el texto del presente trabajo de titulación no podrá ser cedido a ninguna empresa editorial para su publicación u otros fines, sin contar previamente con la autorización escrita de la Universidad.

Asimismo, autorizo a la Universidad que realice la digitalización y publicación de este trabajo de integración curricular en el repositorio virtual, de conformidad a lo dispuesto en el Art. 144 de la Ley Orgánica de Educación Superior

Urcuqui, diciembre del 2020.

_____

Bryan Stalin Herrera Romero

CI: 1724426950

Dedicatory

Thank you God for never abandoning me and allowing me to end this stage of my life with your blessing.

To my mother for her infinite love and support that she has given me every day. For his example of effort and sacrifice that have always made proud.

To my father for his unconditional support and his advice that has allowed me to be a better person. For instilling in me the value of effort and dedication in everything I do.

To my brothers Gaby, Franklin and Pamela for always be there when I need you, for your example of kindness and sincerity and for the happy moments that fill my heart.

To my nephews Adriana, Dilan and Johan for making my life more fun and always allow me to share your follies with you.

To my aunt Sandra because you are like my second mother.

To my grandmother Rosita who I know is taking care of me from heaven, this is for you.

Finally, to all my family in general for allowing me to be part of you and share wonderful moments that I would not change for anything.

Bryan Stalin Herrera Romero

Acknowledgements

I would like to offer my sincere thanks to my advisor, PhD. Graciela Salum, for her support, guidance and patience during the development of this research project. In addition, to always be aware of our education and instill in us those little doubts that always make us want to know more.

I would like to thank Professor Paola Echeverría for her advice and suggestions in the development of the software. Similarly, I would like to thank PhD. Oscar Chang for his support in the development of the thesis.

I would like to thank the members of the jury, PhD. Markus Tellkamp and MSc. Fernando Villalba for their suggestions in the benefit of my thesis.

I want to thank all my teachers for their warmth and patience in teaching throughout these years.

To all my friends with whom I shared unforgettable moments and who allowed me to learn new things every day. Especially on outings to eat.

To Jhon for his friendship since we met.

To Johanna for advising me in the development of my thesis.

To all my sports friends who taught me to never give up despite obstacles.

Finally, to my dear Yachay Tech University, its professors and staff for allowing me to feel at home.

Bryan Stalin Herrera Romero

Resumen

En Ecuador, la diabetes es una de las enfermedades más notorias, posicionándose como la segunda causa de muerte (solo después de las cardiopatías isquémicas) con prevalencia en la población de 10 a 59 años. Uno de cada 10 ecuatorianos mayores de 50 años padece de diabetes y aproximadamente el 30% de estas desarrolla complicaciones visuales. La retinopatía diabética es responsable del 10% de nuevos casos de ceguera cada año. Sin embargo, un diagnóstico precoz de esta patología puede ayudar a ofrecer un tratamiento adecuado y oportuno. El fondo de ojo es un lugar rico en información para el diagnóstico de varias enfermedades oculares. Tener acceso a instrumentación oftálmica capaz de capturar y analizar imágenes del fondo de ojo podría prevenir la pérdida severa de la visión o ceguera mediante un diagnóstico temprano adecuado. Este trabajo de investigación se centra en el diseño y evaluación de una cámara de fondo de ojo portátil, económica y no midriática basada en Raspberry Pi, con el fin de detectar la retina. El prototipo se implementó de acuerdo a ciertas normas ISO. Además, en este trabajo se desarrollaron dos sistemas para la detección de retinopatía diabética en dos lenguajes de programación: MATLAB y Python. El primero se centra en el pre-procesamiento, segmentación, extracción de características y el análisis de la patología identificada, mientras que el segundo se centra en la extracción de características de una imagen digital para crear una clasificación multiclase con la finalidad de detectar la presencia o ausencia de retinopatía diabética mediante el uso de redes neuronales convolucionales. Finalmente, se considera que los resultados obtenidos se pueden mejorar en trabajos futuros, tanto para el prototipo de cámara no midriática como para el software desarrollado.

Palabras clave: Diabetes, retinopatía diabética, cámara no midriática, análisis de imágenes, diagnóstico temprano.

Abstract

In Ecuador, diabetes is one of the most notorious diseases, positioning itself as the second cause of death (only after ischemic heart diseases) with prevalence in the population aged 10 to 59. One of each 10 Ecuadorians over 50 years of age suffers from diabetes and approximately 30% of these develop visual complications. Diabetic retinopathy is responsible for 10% of new cases of blindness every year. However, an early diagnosis of this pathology can help to offer an adequate and timely treatment. The fundus is a rich place of information in the diagnosis of several ocular diseases. Having access to ophthalmic instrumentation capable of capturing and analyzing fundus images could prevent severe loss of vision or blindness through a suitable diagnosis. This research work is focused on the designed and evaluation of a portable, inexpensive, non-mydriatic fundus camera based on Raspberry Pi, in order to detect the retina. The prototype was implemented according to certain ISO standards. Furthermore, in this work two systems for the detection of diabetic retinopathy were developed in two programming languages: MATLAB and Python. The first is focused on preprocessing, segmentation, feature extraction and the analysis of the identified pathology, while the second is focused on feature extraction of a digital image to create a multiclass classification in order to detect the presence of absence of diabetic retinopathy through the use of convolutional neural network. Finally, it is considered that the results obtained can be improved in future work, both for the non-mydriatic camera prototype and the software developed.

Keywords: Diabetes, diabetic retinopathy, non-mydriatic camera, image analysis, early diagnosis.

INDEX OF CONTENT

INDEX OF FIGURES

INDEX OF TABLES

INDEX OF ANNEXES

ABBREVIATIONS

DR	Diabetic Retinopathy
OHT	Ocular Hypertension
OAG	Open-angle glaucoma
CRVO	Central Retinal Vein Occlusion
mm	Millimeters
um	Micrometer
°	Degrees (angle)
V	Voltage
mAh	Milliampere hour
ISO	International Organization for Standarization
CAD	Computer-aided Diagnosis
RGB	Red, Green, Blue
HSV	Hue, Saturation, Value
HIS	Hue, Saturation, Intensity
AI	Artificial Intelligence
NN	Neural Network
ANN	Artificial Neural Network
CNN	Convolutional Neural Network
WHO	World Health Organization
PHO	Panamerican Health Organization
NoIR	No Infrared
GPIO	General Purpose Input/Output

InGaN	Indium gallium nitride
AlGaAs	Aluminium gallium arsenide
LCD	Liquid Crystal Display
STARE	Structured Analysis of the Retina
ReLu	Rectified Linear Unit
TP	True Positive
TN	True Negative
FP	False Positive
FN	False Negative

CHAPTER 1

1. INTROUDCTION

This chapter describes the theory found and employed in this thesis with the objective to know and understand the field of study on which this research work will focus. It consists of the development of concepts to introduce the topic of physiology of the eye, retina pathologies, current diagnosis methods and eye exam, digital image processing and others.

1.1. Human Vision

The ocular system is one of the most important senses in human beings. Sensory cells and associated tissues are responsible for providing vision (1,2). It is by far the most used of the five senses because it allows gather information from our surroundings. More than 75 percent of the information we receive about the world around us consists of visual information (1,2). The anatomy of the eye is comprised by three regions. The outer region of the eye consists of the cornea and sclera, the middle region consists of the iris, ciliary body and choroid, while the inner region is the retina (Figure 1) (2). In addition, the eye is constituted by two water-like fluids. First, aqueous humor is what fills up the anterior and posterior chamber of the eye. This is produced by the ciliary body and is also responsible for maintaining the shape of the eye (1,2). Second, vitreous body is a semisolid gel structure, remarkable for the small amount of solid matter that it contains. The solid material is made up of a form of collagen, vitrosin, and hyaluronic acid (1,2). Having information about the physiology of the retina is of great importance for the diagnosis of different diseases specific to the ocular system (3).
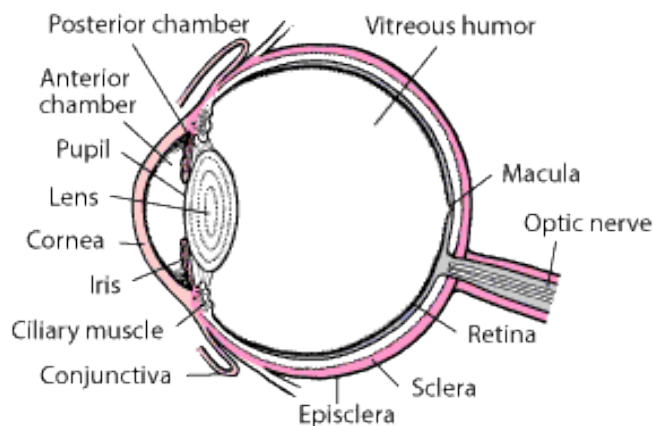
Figure 1. Anatomy of the Eye. Source: (2)

1.2. Retina

The retina is a thin multilayer consisting mainly of neuronal cells (4). Much like the film of a camera, the retina receives, modulates and transmits visual stimuli from the environment to the optic nerve (visual cortex of the brain) (4,5) and, therefore, it has been considered as an extension of the central nervous system within the eye (6).

The retina is divided into nine layers: outer and inner segments of photoreceptors (rods and cones), external limiting membrane, outer nuclear layer, outer plexiform layer, inner nuclear layer, inner plexiform layer, ganglion cell layer, nerve fiber layer and internal limiting membrane (Figure 2) (4).
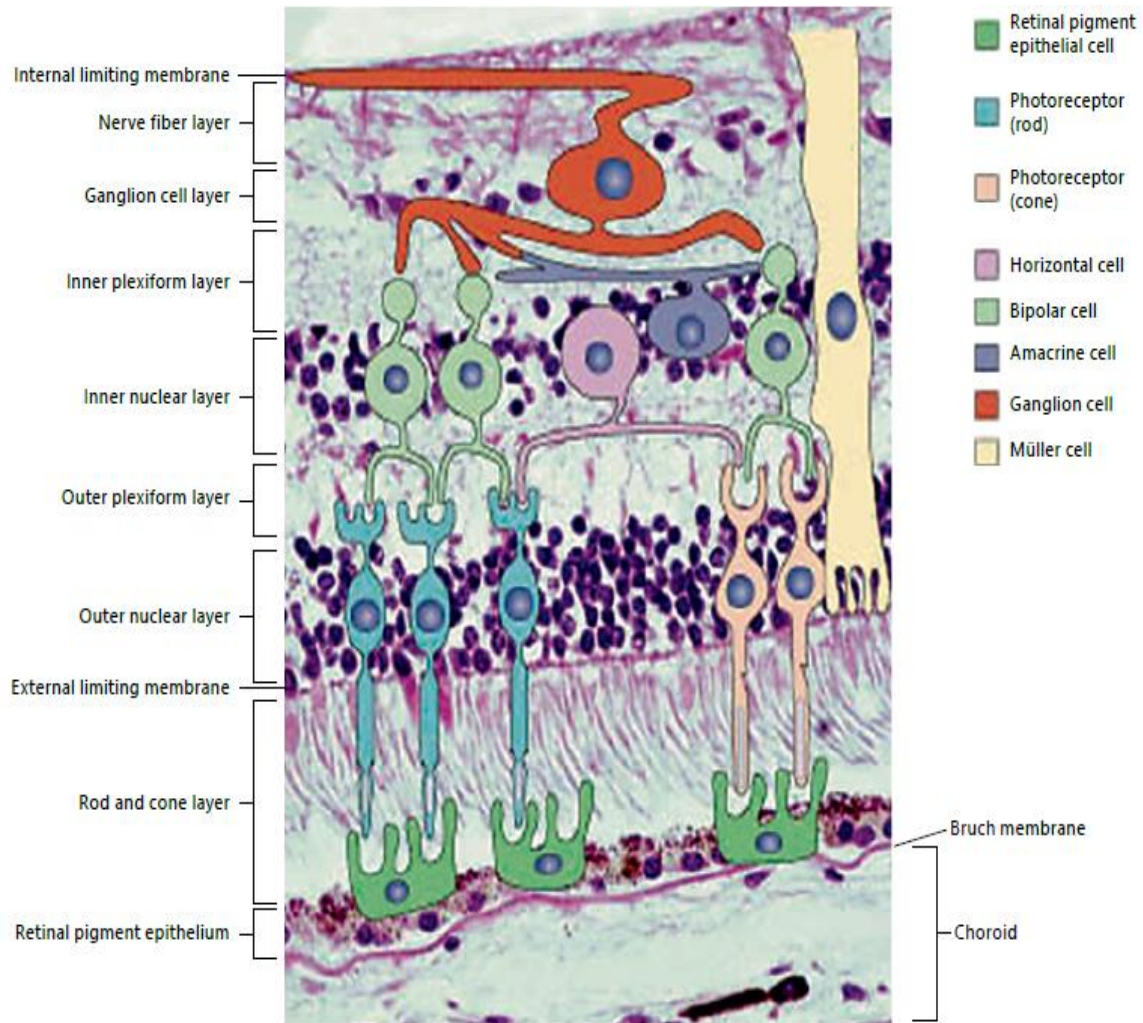
Figure 2. Photomicrograph of the retina. Source: (4)

In addition, there are several components that make vision function. Among the main are: macula, fovea, optic disk and blood vessels. Macula is a small area in the center of the retina that allows seeing detailed images (7). Fovea is a small depression in the center part of the macula where visual acuity is highest (7). Optic disk is a circular shaped anatomical structure with a bright appearance that lack sensory cells (8). Blood vessels are the central retinal artery and vein and their branches. The arteria centralis and its accompanying vein pierce the optic nerve (Figure 3).
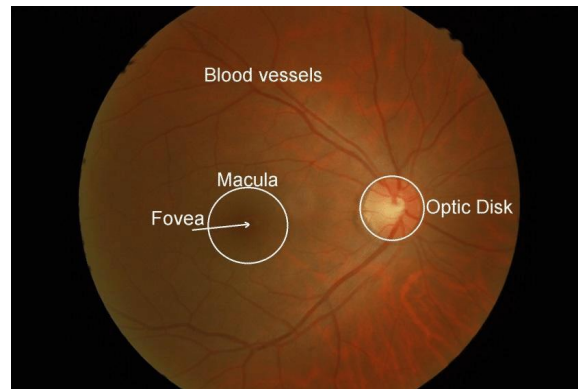
Figure 3. Retinography showing the location of macula fovea, optic disk, blood vessels. Source: (8)

1.3. Retina Disorders

As illustrated above, the retina is an extremely complex structure subjected to a broad spectrum of retinal pathologies and in some cases vision loss (4). The capacity of retinal tissue to respond to such injuries depends largely on the specific cells and tissue involved, as well as the type, duration and severity of the injury (4). Some of the more common conditions are described below:

1.3.1. Glaucoma

It is a group of diseases that produce loss of vision or blindness because the optic nerve is gradually destroyed due to high intraocular pressure, a condition called ocular hypertension (OHT) (10). The most common form of glaucoma is known as open-angle glaucoma (OAG), which occurs when the fluid of the anterior chamber reaches the angle between the cornea and iris. Due to the increase in the amount of fluid, the pressure inside the eye rises to level that the optical nerve may be damaged (10).

1.3.2. Age-Related Macular Degeneration

This disease is characterized by clumps of yellowish material (drusen) accumulated within and beneath the RPE cells which may die, or they interfere with photoreceptors, resulting in loss of vision (10). If the photoreceptors in the macula are damaged, it can seriously affect the visual acuity, known as dry macular degeneration (10). However, the more advanced and damaging kind of eye disease is known as wet macular degeneration, in which new blood vessels grow beneath the retina to supply more oxygen and nutrients. The problem is that, they grow in areas where they should not be, for example in the macula, and thus they affect the photoreceptors impairing vision (10).

1.3.3. Retinal Vein Occlusion

This condition develops from a blood clot or blockage of the central vein that drains blood from the retina. It usually affects adults over 50 and occurs in one eye. CRVO often causes macular edema and stimulates the growth of abnormal new blood vessels which lead to blurred vision (7).

1.3.4. Retinal Detachment

This abnormality of the eye is produced when the retina pulls away from its supporting tissue (back of the eye), and the retina fails to function properly when it is separated from its blood supply (7). Several factors are the responsible of this condition, whose symptoms include floaters in the eye, flashing light and a shadow on the side of the eye that may progress towards the center of vision. Retinal detachments must be evaluated and treated as soon as possible (7).

1.3.5. Hypertensive Retinopathy

A retinal analysis is able to diagnose hypertensive problems in a person as high blood pressure can damage the blood vessels of the retina, limit its function and cause vision problems (11, 12). Therefore, the retina can be significantly affected for the following reasons: damage to the nerves of the eye due to poor circulation, blockage of the arteries that supply blood to the retina and blockage of the veins that carry blood that leaves the retina (11). It is of great importance because high blood pressure is one of the greatest risk factors for cardiovascular diseases which is the leading cause of mortality worldwide. Hypertension is responsible for 54% of strokes and 47% of coronary heart diseases (13, 14).

There are several complications if the hypertensive retinopathy is not treated properly, such as: ischemic optic neuropathy, retinal artery occlusion, retinal vein occlusion, damage of the nerve fibers and malignant hypertension. The diagnosis of ocular diseases in people who suffer from high blood pressure is very difficult because they do not show symptoms until the conditions have clearly progressed, explaining why this condition is so dangerous (15). Current investigations are focusing on prediction models of vascular risks through the analysis of images of the fundus, with favorable results (16).

1.3.6. Diabetic Retinopathy

It is a complication of diabetes and one of the leading causes of blindness (17). Diabetic microangiopathy affects the retina early and specifically, showing alterations such as microaneurysms, hard or soft exudates, microhemorrhages, venous dilations and microvascular anomalies (18). Therefore, diabetic retinopathy occurs when high blood glucose levels damage the small blood vessels in the retina. In some people, blood vessels may swell and leak fluid while in other people, abnormal new blood vessels grow on the surface of the retina (19). A comparison between normal retina and diabetic retinopathy is show in Figure 4.
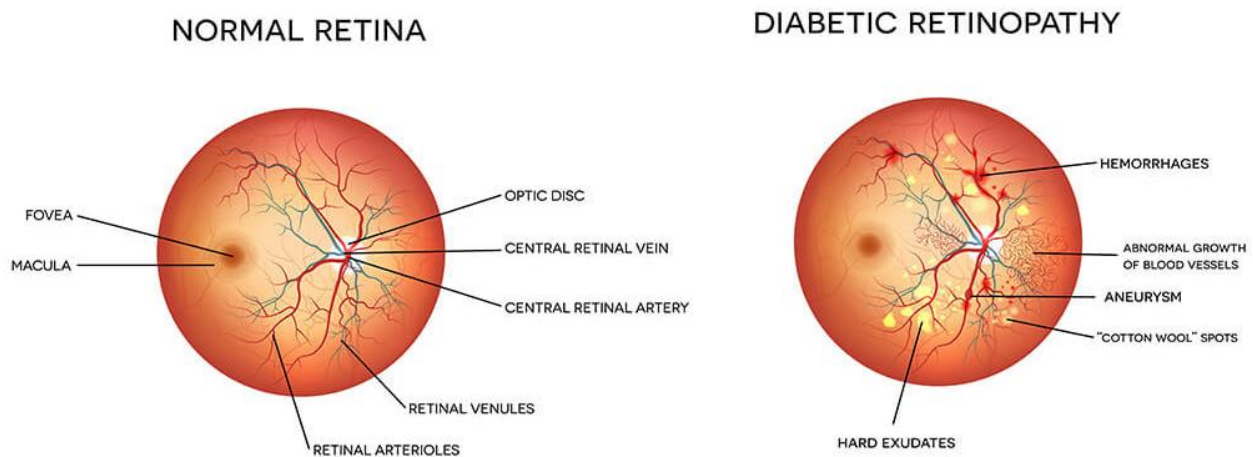
Figure 4. Normal Retina (left) in comparison to Diabetic Retinopathy (right). Source: (19)

Diabetic retinopathy goes through different stages depending on the characteristics that are visualized in the retina: 1) Stage I: Normal Eye. 2) Stage II: Mild Non-Proliferative DR. 3) Stage III: Moderate Non-Proliferative DR. 4) Stage IV: Severe Non-Proliferative DR. 5) Stage V: Proliferative DR (Table 1) (20).

Table 1. Representative stages of Diabetic Retinopathy and its main characteristics. Source: (20)

Stage	Characteristics	Severity
I	- No abnormalities identified	No DR
II	- Micro-aneurysms only	Mild NPDR
III	- Micro-aneurysms - Retinal dot and blood hemorrhages - Hard exudates or cotton wool spots	Moderate NPDR
IV	- More than 20 intra-retinal hemorrhages - Definite venous beading - Prominent microvascular abnormality	Severe NPDR
V	- Neovascularization - Vitreous pre-retinal hemorrhage	Proliferative DR

1.4. Ocular Examination

Currently, eye examinations include a set of techniques that allow the observation of different structures of the eye in order to diagnose or check the progress of a pathology. Medical imaging plays an essential role at the moment of recording the results obtained after a clinical examination (21). In fact, the diagnosis can be made from images acquired using various types of equipment such as: slit lamp photography, specular microscopy, fluorescein angiography, optical coherence tomography, non-mydriatic cameras (22, 23).

1.4.1. Slit-Lamp Photography

It is a variation of the slit-lamp bio microscope used to illuminate and examine structures in the eye at magnification up to 40x (24). It is a technically and aesthetically challenging discipline that requires a good understanding of composition, magnification, precise exposure control, principles of light (direct and indirect) and pathology understanding (24). The first model was presented by Alvar Gullstrand in 1911 and it helped to understand the functioning of the eye and the main pathologies (24).

1.4.2. Fluorescein Angiography

This technique is used in the diagnosis and treatment of retinal disorders and is focused on identifying patterns of vascularity present in the retina through the intravenous injection of sodium fluorescein. This in vivo technique was developed by two Indiana University students in 1960, used is particularly for the treatment and diagnosis of diabetic retinopathy and macular degeneration (24, 25).

1.4.3. Optical Coherence Tomography

This is an imaging procedure recently used for the diagnosis of various retinal pathologies as it provides direct cross-sectional images of the macula, the retinal nerve fibers and the optic nerve. The utility of this technique was demonstrated for the first time in 1991 in the detection of holes, edema, sub-retinal fluids and accumulations of visual pigments (24, 25).

1.4.4. Ophthalmoscope

Ophthalmoscopes are instruments used to observe the fundus and identify possible disease conditions of the human eye (26). This type of instrument, in order to observe the fundus of the eye, uses an external light source to illuminate the retina. This type of equipment looks like a simple optical system, but the ingenuity of its design consists of illuminating and observing the fundus at the same time (26). Two types of ophthalmoscopes are used, direct and indirect.

1.4.5. Fundus Cameras

The operating principle of fundus cameras is based in same idea of an ophthalmoscope but they have the advantage of acquiring images of the fundus digitally, allowing documentation, monitoring and diagnosis of several diseases (26). The illumination system illuminates a homogeneous area of the retina without damaging the image of the fundus due to unwanted reflections (26). This type of camera can be distinguished in two groups:

- **Mydriatic Fundus Cameras**

On one hand, mydriatic cameras require patient's pupils to be dilated. In order to have a good photography of the fundus with a field of 45°, the pupil must be at least 4 mm wide diameter (26). Therefore, it is an easy method of image capturing. However, the use of the drops may be uncomfortable to the patient as it requires a waiting time of approximately twenty minutes for

dilation after administrating medicated eye drops, and the patient may experience blurred vision and hypersensitivity to light (26).

- **Non-mydriatic Fundus Cameras**

On the other hand, non-mydriatic cameras do not require dilation of the pupil. These cameras use the eye's own natural mechanisms of adaptation to light by dilating the pupil under low light conditions (physiological dilation in dark room) (26). Non-mydriatic cameras are designed to continuously illuminate the pupil with infrared light before taking the picture with a flash of white light. This pulsed light can be produced with xenon flash or LED (26).

1.5. International Standards

Although there are a wide range of fundus cameras today, international standards set forth the minimum requirements for cameras to be considered safe and of adequate quality (26). According to the International Organization for Standardization (ISO), the most important fundus camera standards are described in Table 2.

Table 2. ISO Standards for Ophthalmic Instruments. Source: (27,28)

ISO Standards	Description
ISO 10940:2009	- Ophthalmic instruments. Requirements for fundus cameras operation.
ISO 15004-1:2007	- Ophthalmic instruments. Fundamental requirements and test methods. Part 1. General requirements applicable to all ophthalmic instruments
ISO 15004-2:2007	- Ophthalmic instruments. Fundamentals requirements and test methods. Part 2: Light Hazard Protection

ISO standard 10940:2009, together with ISO 15004-1 and ISO 15004-2, specify the requirements and test methods for fundus cameras to observe, photograph or record electronic images from the fundus of the human eye in order to provide a diagnosis (27, 28). In addition, the

most important requirements described in the ISO 10940: 2009 are the optical properties of fundus cameras and safety of light in the eye.

1.5.1. Optical Properties

ISO 10940: 2009 determines that the optical properties to be considered in fundus cameras are: the optical resolving power of the camera, field angle observation, image magnification and pixel size on the retina (26, 27).

1.5.2. Eye Safety

ISO 10940: 2009 states that a fundus camera must meet the specified requirements regarding safety. The ISO 15004-2: 2007 is based on the guidelines established by the international commission about the protection against non-ionizing radiation light produced by ophthalmic instruments (26, 27).

1.6. Computer-Aided Diagnosis

With technological advances in all these methods of image capture and digitalization, several systems have been developed that focus on the computer-assisted diagnostic method (called CAD). The objective is to process digital images and highlight the visible sections of interest captured by cameras to offer a pre-diagnosis that supports the final decision of the health professional (29). In addition, CAD methods require extensive knowledge of machine learning algorithms, a branch of computer science that provides computers the ability to detect clinically significant objects from medical images without the need of an explicit programming algorithm (29).

Digital image processing and analysis represents the area of engineering that focuses on the recognition and detection of certain important properties such as: size, shape, texture, edges, lines, and/or pixel color that reveal important characteristics of 2D or 3D images as well as sequences of various images (30). In fact, an image is defined as a function in two dimensions, where x and y represent the coordinates of a plane, while f (x, y) represents the intensity or gray level. When the coordinates and intensity values are discrete and finite, we speak of a digital image, in which each pixel is coded and described according to the color space that it occupies (31). There are several color models, the main ones being the RGB model, the HSV model and the HIS model.

1.6.1. RGB Model

One of the most used models in computer graphics is the RGB model, since its objective is to create and reproduce colors on monitors or screens (32). The RGB model is represented by a unit cube with the R, G, B axes and their coordinates (1,0,0), (0,1,0), (0,0,1) respectively. The origin (0,0,0) represents the black color, while (1,1,1) represents the white color. Furthermore, it focuses on additive synthesis, where light intensities are added together to obtain different colors (31). The advantage offered by this model is the use of easy and intuitive manipulation tools in filtering, segmentation and process analysis (32).
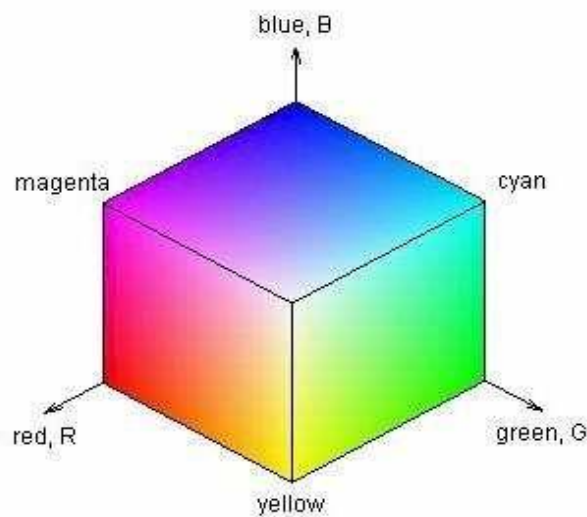
Figure 5. Graphical representation of RGB model. Source: (31)

1.6.2. HSV Model

In the case of the HSV model, whose acronym is derived from the words: Hue (H), Saturation (S) and Value (V), the coordinate system is cylindrical and the subset of this space maintains a pyramid with a hexagonal base that locates the brighter colors (14,16). Using this model, an element with a certain color can be detected, and the influence of the light intensity produced from outside sources can be reduced. Furthermore, this model has the advantage of being invariant to light conditions (16).

Figure 6. Graphical representation of HSV model. Source: (31)

1.6.3. HIS Model

HSI model represents the variables: Hue (H), Saturation (S) and Intensity (I), whereby the hue corresponds to the angle with respect to the red axis, saturation provides a measure of the degree to which a color mixes with white light, and intensity indicates the brightness value of the color (17). The HSI model maintains a non-linear transformation of the RGB color space, modifying the sub-space of the HSV cube, to convert it into two cones joined by a base (14). Currently, this model is an ideal tool to develop image-processing algorithms related to the human visual system.
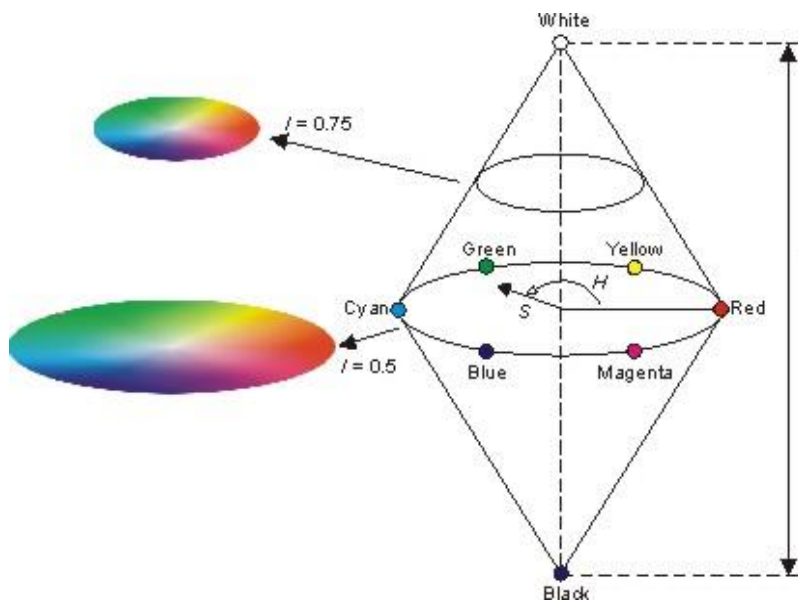
Figure 7. Graphical representation of HIS model. Source: (31)

Therefore, digital image processing and analysis is implemented in response to three major processes regarding images: 1) digitization and encoding, 2) enhancement and restoration, and 3) description and segmentation. The set of solutions is divided into three large groups focused on highlighting, sharpening, contrasting and eliminating noise or unwanted effects in an image (31). These methods can be classified into: a) methods in spatial domain; b) methods in frequency domain and c) feature extraction methods (Figure 8).
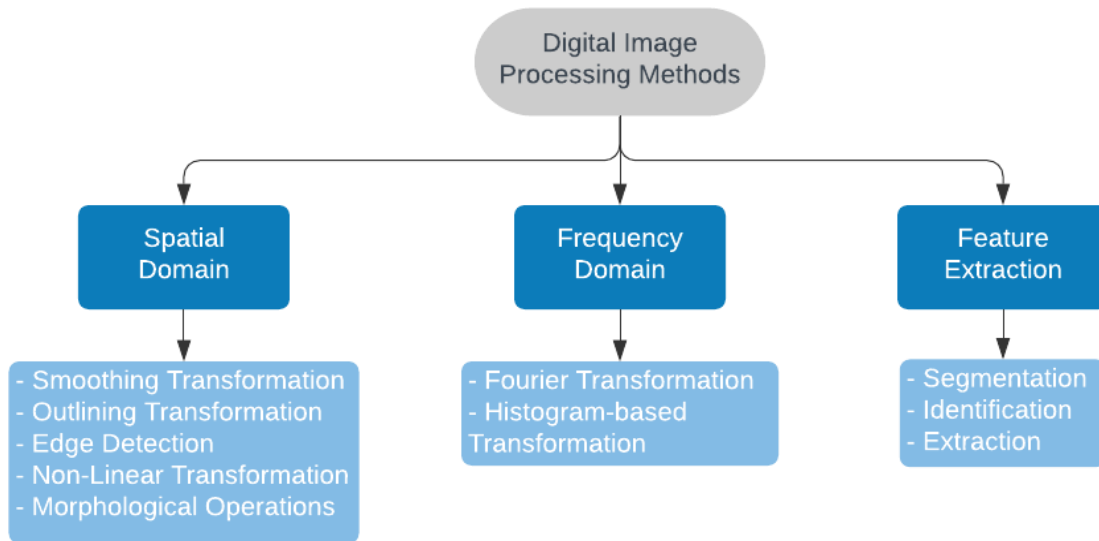
Figure 8. Digital Image Processing Methods

1.6.4. Spatial Domain Methods

The methods in spatial domain are:

1) The smoothing transformation or low-pass filter that attenuates high-frequency components and focuses on smoothing the edges of an image to reduce noise peaks or changes in intensity. The idea is to replace the value of a pixel by the average of the neighborhood to blur the image (33).

2) The outlining transformation allows to highlight and make the variations of color and edges of an image more visible through increasing contrast, and thus improving the blurred appearance of an image (31).

3) Edge detection that provides essential information about the limit of the objects to detect areas that present variations or changes in intensity (34). Among the main algorithms are:

Prewitt filters, Sobel filters and Canny edge detector. The Prewitt edge detector uses masks that differentiate in one direction and average in another, allowing the noise effect to be controlled (36). On the other hand, Sobel uses convolution masks to calculate the gradient in two directions (row and column) (36). Finally, Canny considers three criteria for calculating edges: good detection, good localization and uniqueness of response. The solution is a complex exponential function that approximates the Gaussian function (36).

4) The non-linear transformations allow acquiring the values corresponding to the neighborhood of each pixel and ordering them from highest to lowest, allowing to find the sharpest or darkest points of an image (31).

5) Morphological operations are procedures that provide improvements in images and which fundaments lie in the theory of sets applicable to binary images (36). These procedures are applied for observation and comparison purposes, with the use of non-linear operations, such as: opening and closing, erosion and dilation (31). The objective of implementing the erosion and dilation operations is to differentiate between the foreground structure and the background structure, while the opening and closing processes consist of eliminating structures that are smaller than the structuring element (36). For this reason, the opening and closing processes manipulate erosion and dilation, thereby eliminating and adding foreground structures to the image, respectively (36).

1.6.5. Frecuency Domain Methods

Frequency domain methods mainly focus on the following transformations:

1) Fourier transformation that allows suppressing certain frequencies while not altering the others (37). This type of transformation is used to decompose an image into its sine and cosine components (38).

2) Histogram-based transformations are a graphical representation of the frequency at which the gray levels or intensity appear in each color plane, thus allowing much information in an image to be condensed (37).

1.6.6. Feature Extraction Methods

These represent a system of algorithms that acquires an image as input to extract the necessary attributes of interest (31). The most important process at the time of extraction is based on an image

segmentation procedure since it allows to subdivide the acquired image into different regions, in such a way that each of the pixels in those regions has similar properties or attributes (homogeneity). The algorithms used focus on two basic properties of intensity, discontinuity and similarity (39). Segmentation represents a challenge in image processing, since the progress towards the final result depends on precision and accuracy of segmentation (39).

1.6.7. Digital Image Processing

The procedure designed to indicate important findings on an image allow showing the characteristics of anatomical structures and visible lesions. This is important to keep track of the severity of the disease and assess the progress of treatment over time (40,41). Among the most important are pre-processing, segmentation and extraction of characteristics (Figure 9).
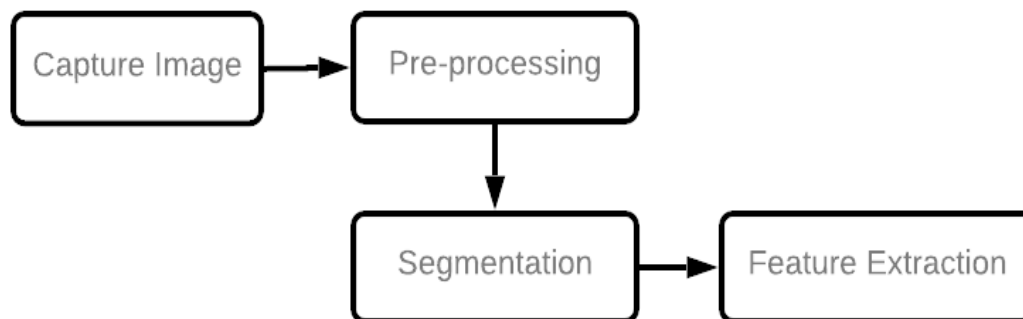
Figure 9. Typical procedure for Digital Image Processing

1. Pre-processing

The pre-processing stage is developed with the objective of increasing the quality of the results, improving the contrast of the image, balancing the color space, highlighting the main characteristics and reducing the environment that is not of interest to the problem (42,43).

2. Segmentation

The segmentation process is one of the most important and used as it is defined as the division of an image into regions or complete objects, recognizing information from each of the fragments of interest present in an image based on the problem to be solved (44,45). The main segmentation

techniques include: region-based segmentation, boundary detection segmentation, and clustering-based segmentation (46).

3. Feature Extraction

Feature extraction is part of a dimensionality reduction process that aims to describe images according to a recognition pattern (47,48). This procedure is carried out to identify, describe, highlight and extract characteristics of the objects of interest such as: shape, position and size, through the use of binary thresholds, implementation of masks and removal of small objects (49).

1.7. Artificial Intelligence

Artificial Intelligence studies different ways to build intelligence programs and machines that can solve problems, usually considered a human prerogative (50). The advantages of AI in medicine are good results in medical fields such as radiology and dermatology, which have similarities to ophthalmology as they are deeply rooted in diagnostic imaging (51). AI is particularly suitable for managing the complexity of ophthalmology: AI can assist clinical practice by using efficient algorithms to detect and learn features from large volumes of imaging data, helping to reduce diagnosis and therapeutic errors (51).

1.7.1. Machine Learning

It is a subfield of artificial intelligence that provides systems the ability to automatically learn and improve from experience without being explicitly programmed (50). It allows us to use devices with computational capacity so that they learn to extract patterns and relationships that exist in the data by themselves (52). Those patterns can then be used to predict behaviors and making decision. It is carried out with the use of different algorithms that help to solve these problems.

1.7.2. Deep Learning

It is a subfield of machine learning which uses neural networks to analyze the importance of different factors using a structure similar to the human nervous system (50). A deep learning architecture consists of multilayer features or stacks of simple modules that are not designed by human engineers, but learned from data using a learning procedure (53).

1.7.3. Neural Networks

Neural networks or more specifically artificial neural networks (ANNs) are used to mimic the human brain through a set of algorithms (54). It consists of a model of interconnected neurons, whose spatial arrangement and linking can be used to solve computer-based application problems in various fields (55). A neural network is comprised of four main components: inputs, weights, a bias or threshold and an output (54). The basic structure can be modeled as shown in figure 10 (46).
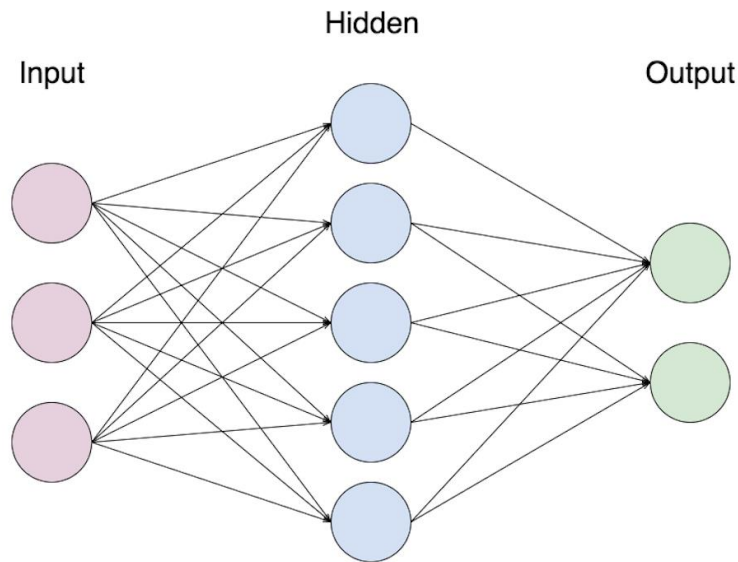
Figure 10. Basic structure of a Neural Network. Source: (56)

1.7.4. Convolutional Neural Network

These are analogous to the traditional ANNs in that they are comprised of neurons that self-optimize through learning (56). From the input of raw image vectors to the final output of the class score, the entire network will express a single perceptive score function (the weight) and the last layer will contain loss functions associated with the classes (56).

The main difference between CNNs and the traditional ANNs is that CNNs are primarily used in the field of pattern recognition within images. This allows us to encode image-specific features into the architecture, making the network (56).

The layers within the CNN are comprised of neurons organized into three dimensions: the spatial dimensionality of the input (height and width) and the depth. With respect to the overall architecture, convolutional neural networks are comprised of three types of layers: convolutional layers, pooling layers and fully connected layers (56) (Figure 11).
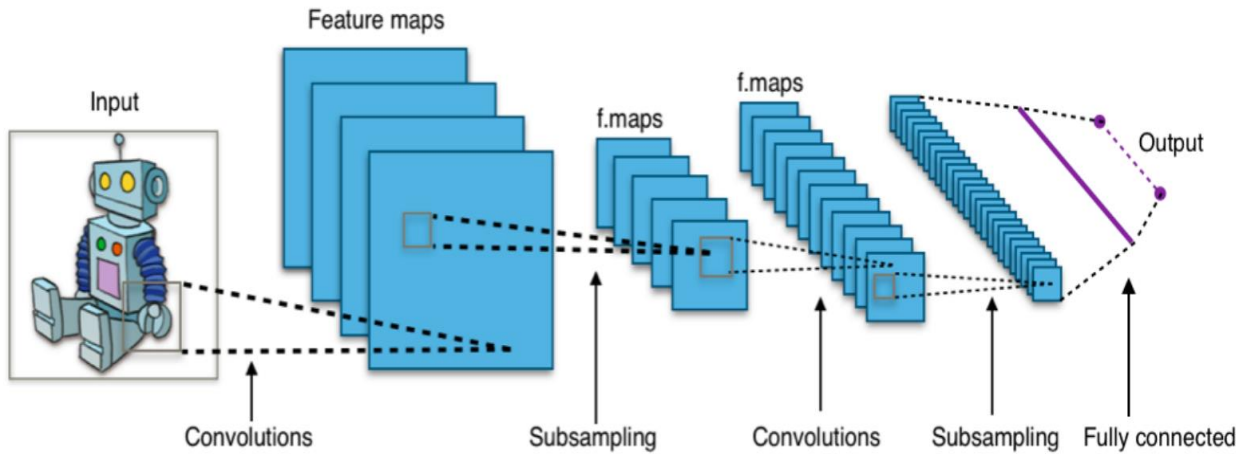
Figure 11. Overall architecture of CNN. Source: (56)

- **Convolutional Layer**

Convolution is a mathematical operation that extracts features from an image taking two inputs into account, image matrix and a filter or kernel (small matrix), usually the first step for further analysis (57). Convolutional layer creates a feature map to predict the class probabilities for each feature by applying this filter to the whole image, few pixels at a time (58,59). The output of the kernels goes through a linear or non-linear activation function, such as: hyperbolic, sigmoid, tangent, SoftMax and others to form the output feature maps (60).
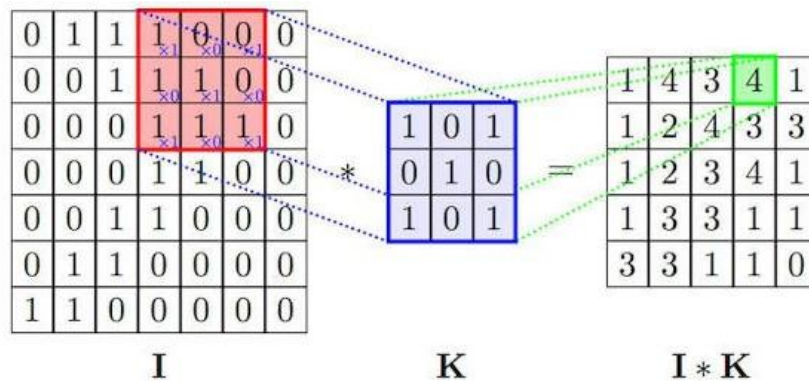
Figure 12. Representation of Convolutional Layer. Source: (60)

- **Pooling Layer**

Pooling layers aim to gradually reduce the number of parameters when the images are too large (57). Spatial pooling also called subsampling or down sampling which reduces the dimensionality of each map but retains important information (56, 57). Spatial pooling can be of different types, Max Polling and Average Pooling (Figure 13). On one hand, Max Pooling returns the maximum value from the portion of the image covered by the Kernel. On the other hand, Average Pooling returns the average of all the values from the portion of the image covered by the Kernel (61).
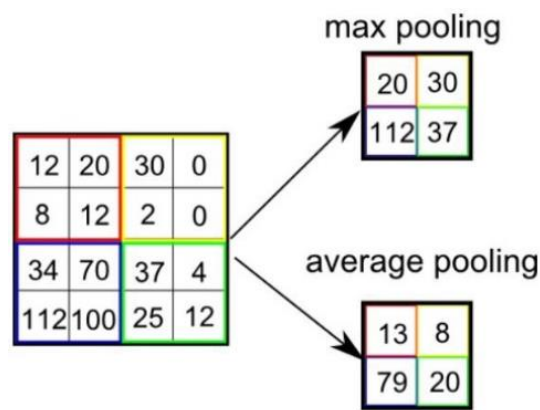
Figure 13. Representation of Pooling Layer. Source: (61)

- **Fully Connected Layers**

Fully connected layer or classification layer computes the score of each class from the extracted features from a convolutional layer in the preceding steps (60). Now that we have converted our input image into a suitable form for our Multi-Level Perceptron, the image will be flattened into a column vector. The flattened output is fed to a feed-forward neural network and backpropagation is applied to every iteration of training. Over a series of epochs, the model is able to distinguish between dominating and certain low-level features in images and classify them using the Softmax Classification technique (61).
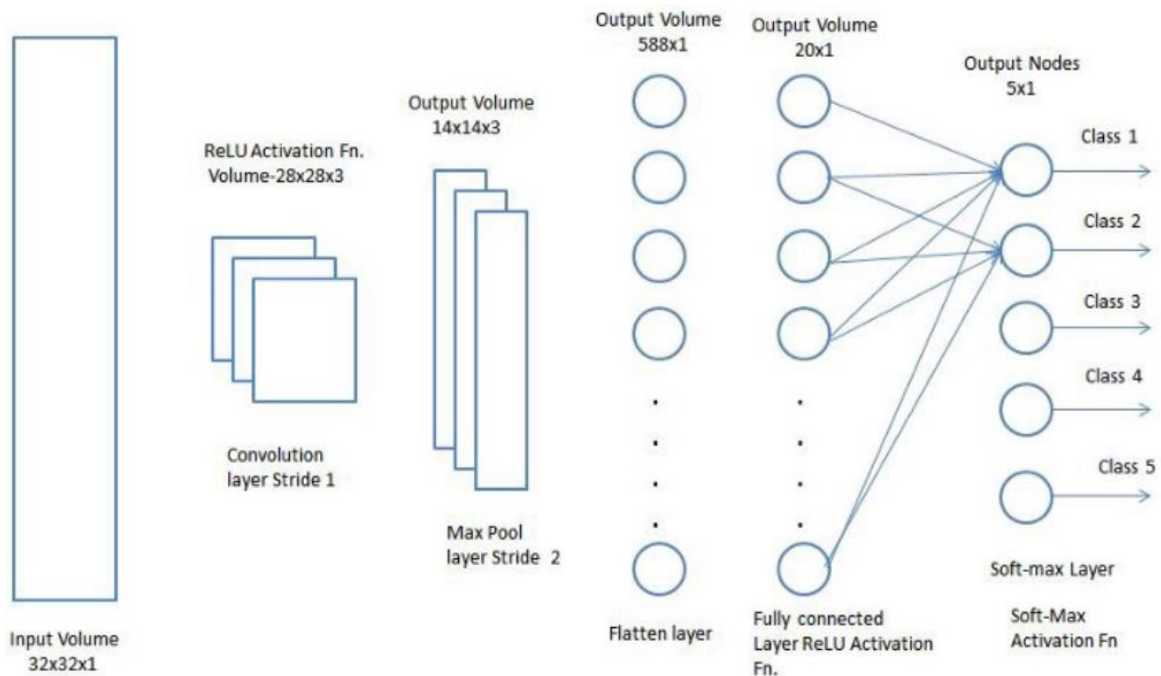
Figure 14. Representation of Fully Connected Layer and Softmax Classification. Source: (61)

1.8. CNN Model Performance

The performance measure is an essential part of machine learning model. It is evaluated on the basis of two important parameters, accuracy and generalization. Accuracy means how well model predicts the right target value and generalization means how well model behaves on seen and unseen data (62).

1.8.1. Confusion Matrix

Confusion matrix or error matrix is a better or complementary method to evaluate the final model (63). This consists of a two-dimensional table (Actual-Prediction) with a set of representative classes in each one. True Positive (TP) is the class of true data and predicted correctly. True Negative (TN) is the class of the data that is false and predicted as such. False Positive (FP) is the class of the data that is false but predicted as true. Finally, False Negative (FN) is the class of the data that is true but the prediction is false (Figure 15) (64).

Figure 15. Model of Confusion Matrix. Source: (64)

The results obtained from implementing the confusion matrix are used to calculate certain parameters related to the validity of the model. These parameters are:

- **Accuracy:** It is the number of all correct predictions (64).

$$ACC = \frac{TP + TN}{TP + TN + FN + FP}$$

- **Error Rate:** It is the number of all incorrect predictions (64).

$$ERR = \frac{FP + FN}{TP + TN + FN + FP}$$

- **Sensitivity (Recall):** This metric tells us how accurately the positive classes were classified as positive (64).

$$SN = \frac{TP}{TP + FN}$$

- **Specificity:** This metric tells us how accurately negative values are classified as negative (64).

$$SP = \frac{TN}{TN + FP} :$$

- **Precision:** Focuses on determining predicted positive values that are actually positive values (64).

$$PREC = \frac{TP}{TP + FP}$$

In addition, other classification accuracy indicators can be evaluated from confusion matrix (65). This is the case of Cohen's Kappa, a statistical coefficient that represents the degree of accuracy and reliability in a statistical classification and allows assessing the percentage of concordance between variables (66). In order to interpret the statistical significance from Kappa values are suggested as follows: 0.01 to 0.20 represents slight agreement, 0.21 to 0.40 represents fair agreement, 0.41 to 0.60 represents moderate agreement, 0.61 to 0.80 represents substantial agreement and 0.81 to 1 is almost perfect or perfect agreement (66). The formula used to calculate this value is:

$$k = \frac{p_o - p_e}{1 - p_e}$$

where p_o is the relative observed agreement among raters, and p_e is the hypothetical probability of chance agreement (66).

1.9. Purpose and Research Question

The purpose of the present research is to develop and evaluate a prototype of non-mydriatic camera to offer an accurate and successful capture of retinal images. In addition, to implement a digital image processing and analysis software to identify each part of the retina, detect anomalies and classify them depending on the presence or absence of diabetic retinopathy by using convolutional neural network. I hope this will help to reduce the number of patients with vision loss as consequence of the diabetes in the country.

CHAPTER 2

2. PROBLEM STATEMENT

The second chapter is going to present the background of this topic in the international and Ecuadorian context. The main issues regarding the health of the population, statistical data relating to the disease, and the importance for the development of new diagnostic methods are discussed.

2.1. Background and Problem Discussion

Diabetes is a serious chronic disease that occurs when the pancreas no longer produces enough insulin (a hormone that regulates the level of sugar or glucose in the blood), or when the body can no longer use the insulin that it produces (67). The International Diabetes Federation published the ninth edition of its Diabetes Atlas in order to detail the significant growth of the disease, which has tripled in the last 20 years. It has increased from an estimated 151 million people with diabetes in 2000 to 463 million at the onset of 2020. All of this makes diabetes the fastest growing health problem this century (68).

The first World Report on Diabetes published by World Health Organization highlights the enormous scale of the problem, and suggests actions to reverse current trends (67). The prevalence of diabetes has increased faster in low- and middle-income countries than in high-income countries, becoming major cause of heart attack, blindness, kidney failure, stroke and lower limb amputation (69). The main ocular condition associated with diabetes is diabetic retinopathy, which is responsible for 1.8 million of the 37 million cases of blindness worldwide (70,71).

In Ecuador, diabetes is the second cause of death only after ischemic heart diseases. According to the Panamerican Health Organization (PAHO) the prevalence of diabetes in the population aged 10 to 59 is 1.7% (72). In Ecuador, one out of 10 people over 50 years of age suffers from diabetes and approximately 30% develop visual complications due to this disease (72,73).

DR is responsible for 10% of new cases of blindness every year, with 1.6% of diabetic patients being legally blind, since the risk of blindness in diabetic patients is approximately 25 times greater than the rest of the population (74). As the incidence of diabetes gradually increases, there is the

possibility that more individuals will suffer from eye complications, which, if not properly managed, may lead to permanent eye damage (74).

Therefore, DR is characterized by a group of lesions found in the retina of individuals suffering from diabetes mellitus. The abnormalities that are developed during diabetic retinopathy occur in a predictable progression, with minor variations, in the order of their appearance (75). So, detecting and treating the disease in early stages is the best way to control diabetic eye disease and concomitant vision loss or blindness.

The most important means to prevent DR is to have frequent check-up with the ophthalmologist. Therefore, for the health professional it is of utmost importance to use modern medical devices and methods of analysis that would allow for an early detection of the disease. In a panel organized by the national assembly in 2017, Virginia Gomez de la Torre, spokeswoman for the health platform, said that: "it is important to change from a curative approach, which contemplates a concept of pathological and medicalized medicine, to a preventive vision of diseases" (76).

CHAPTER 3

3. OBJECTIVES

3.1. General Objective

To detect the presence of diabetic retinopathy in early stages of the disease through the development of hardware for the capture of images of the retina and the design of corresponding software for the processing, analysis, and classification of digital images.

3.2. Specific Objectives

- To develop a portable and inexpensive image capturing device to evaluate the retina.
- To design software for the processing and analysis of fundus digital images using mathematical morphology.
- To implement an automatic software based on convolutional neural networks to evaluate the presence or absence of diabetic retinopathy features.

CHAPTER 4

4. METHODOLOGY

This section describes the methodology used in order to create a camera prototype and a method for the early detection of diseases in the retina using image analysis. This approach led to the design and implementation of hardware (non-mydriatic camera for detection of retina) and software (image processing and pathology detection). First, the materials, components and processes that were carried out for the development of the non-mydriatic camera prototype are described. Second, a description of the strategies, programs and libraries used for the development of the necessary algorithms is presented.
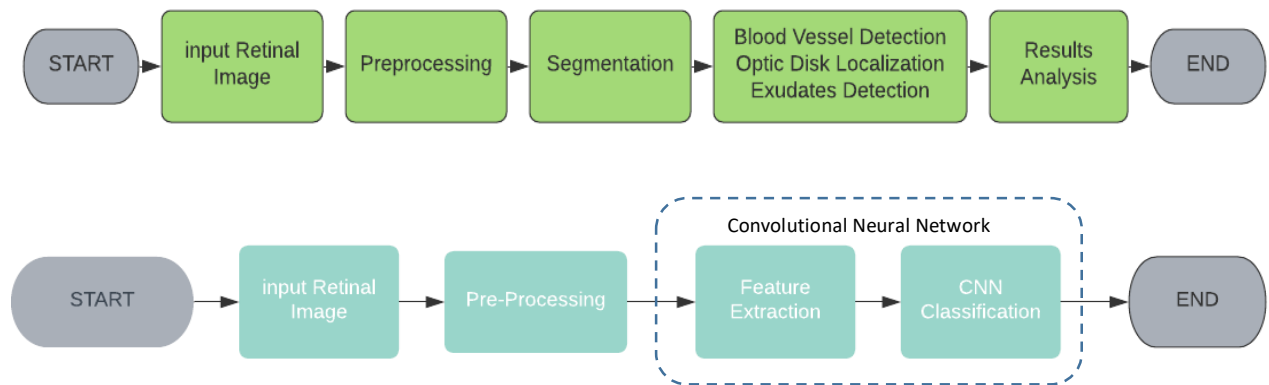
Figure 16. General Flow Charts of Processing and Analysis of digital images (up) and Classification of digital images (down).

4.1. Camera Hardware for Retina Detection

The proposed hardware in this thesis is a non-mydriatic camera as it does not require the use of drops to dilate the pupil.

4.1.1. Components

The non-mydriatic camera prototype uses various electronic and ophthalmological components, as shown in Table 3. In order to develop this prototype, it was necessary to combine: Raspberry pi 3 Model b+, NoIR camera board, infrared and white dual LED, LCD touchscreen, and an ophthalmological lens as the main used components.

Table 3. List of Components for Non-mydriatic camera

Component	Amount
Raspberry pi 3b+	1
NoIR Camera	1
Dual LED	1
LCD Touchscreen	1
SD Card	1
Battery	1
Shutter Button	1
Resistor	1
Micro-USB Cable	2
HDMI cable	1
Jumper Cables	5
Condensing Lens	1

- **Raspberry Pi 3 b+**

The Raspberry Pi Model 3b+ is a computer board, similar in size to a credit card that easily interacts with its environment (77). Among its main features, it has a Broadcom BCM2837B0 processor, requires a 5V power supply and allows connectivity through Wireless LAN, Bluetooth, Ethernet, USB ports or GPIO pins. Given its capacity, it offers the best quality audio and video inputs that can be stored on an external SD card (Figure 17) (78).
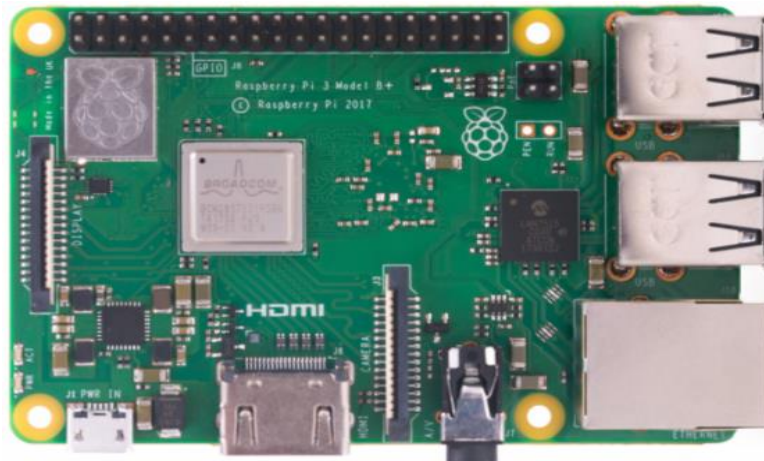
Figure 17. Raspberry Pi 3 b+. Source: (78)

Unlike other devices such as Arduino or FPGA, the main advantage that the Raspberry offers to the present project is its similarity in characteristics with respect to a computer in both hardware and software design. Therefore, a comparative analysis between Raspberry Pi 3 b+, Arduino board and FPGA was implemented (Table 4).

Table 4. Advantages of Raspberry Pi 3 b+ with respect to FPGA chip and Arduino Microcontroller. Source: (79,80)

Basis of Comparison	Raspberry Pi 3 b+	FPGA	Arduino
About and Definition	It is a series of single-board computers (compatible to some operating systems) with low cost, which plugs into a computer monitor or TV. It allows the use of standard keyboard and mouse to operate it.	Field-Programmable Gate Array can be configured by the user after manufacturing (unlike traditional CPU). It is an integrated circuit (chip) customized for a specific application.	It is a microcontroller motherboard (simple computer) in that, only one program can be run at a time. Also, it is a prototype platform based on hardware and software great for quick setups.
Connectivity Abilities	It can be connected to Bluetooth devices and Internet using Ethernet or by connecting to Wi-Fi.	It requires the use of a development card in order to have Bluetooth and internet connection.	It cannot connect to Bluetooth devices and Internet without a Shield.
Ports Availables	It contains an HDMI port, audio port, 4 USB ports, camera port, and LCD port to help in media applications.	FPGA chip does not have any of the ports like a microcontroller. However, a development card with a FPGA device can provide multiple ports.	Arduino does not have any of the ports on the Microcontroller board, but it can be achieved by using Shields.
Board Applications	Performs multitask several programs with its Broadcom BCM2837, means to build a complex project with multiple actions at a time.	It includes a variety of applications for digital signal processing, device controllers, bioinformatics, ASIC prototyping, medical imaging and many more.	It cannot be achieved in Arduino since Microcontrollers have only 16 MHz.
Areas of Usage	It is used when a user requires fully-fledged computer means and wants to control more complicated projects, performing multiple tasks.	It has a wide variety of field applications such as: telecommunications, data centers, scientific computing, audio and video processing.	Arduino microcontroller board can be used for simple and repetitive tasks

- **Infrared Camera Module V2**

The Infrared Camera Module v2 (Pi NoIR) has an 8-megapixel sensor, similar to a smartphone camera, is sensitive to infrared light, and has a fixed focus (Figure 18). Therefore, it offers the same features as a regular camera with only one difference: infrared camera module does not employ an infrared filter. This means that pictures taken by daylight will look decidedly curious, but the ability to see in the dark with infrared lighting will increase (81).
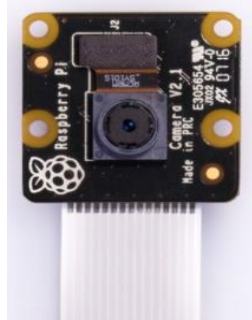
Figure 18. . Infrared Camera Module v2 (Pi NoIR). Source: (81)

Figure 19. Coaxial white and infrared dual LEDs (SMT47W/850). Source: (82)

- **LED (SMT47W/850)**

The most important components are the coaxial white and infrared dual LED (SMT47W/850), manufactured by Ushio Ipex Incorporated and distributed by Marubeni Corporation (77). The model used is an InGaN/AlGaAs material chip, 400 μm x 400 μm in size with a white wavelength peak of 850nm. This type of LED is used specifically for ophthalmoscopy, as it allows the illumination of the retina (Figure 19) (82).

- **External Battery and LCD**

Among the additional components are (see Figures 20 and 21):

1) An external lightweight lithium battery of 10000mAh as the power source for all electronic components. The advantage of this type of battery lies in its dual USB charging capability, in addition to offering a 5V output (83).

2) A 7-inch touchscreen display with a 1024x600 resolution capacitive screen and IPS display panel. It is characterized by its easy adaptation to the Raspberry Pi operating system (84).

Figure 20. Havit External Battery. Source: (83)
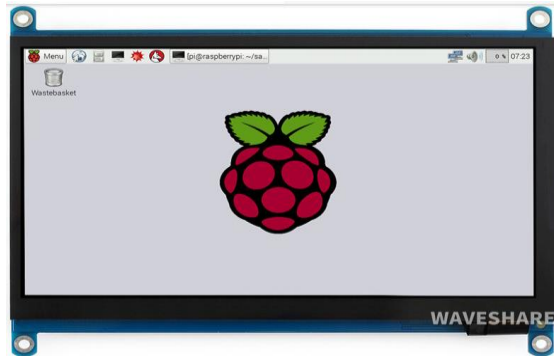
Figure 21. Waveshare 7" Touchscreen. Source: (84)

4.1.2. Prototype Development

The figure 22 shows the graphical representation of the process implemented for the development of the non-mydriatic camera prototype with each of the procedures, configurations, connections and electronic components used.
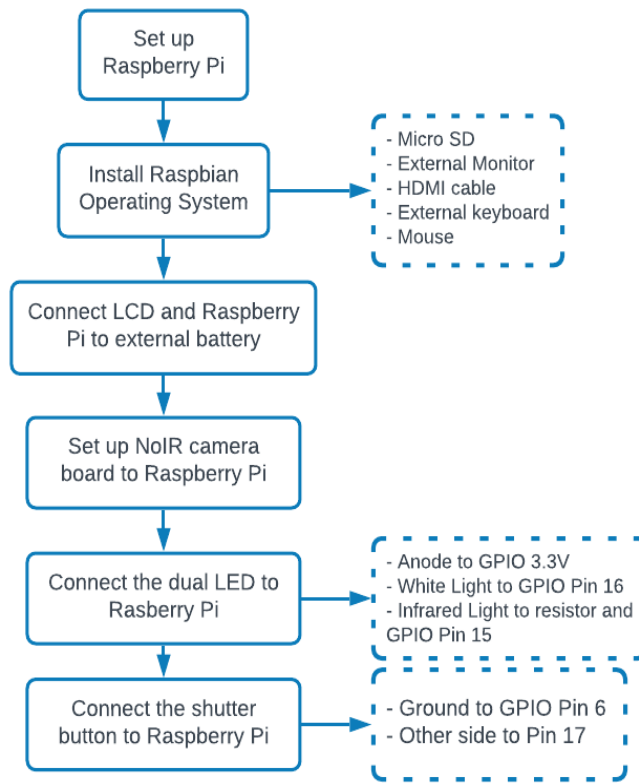
Figure 22. Description for Hardware Development

First, it is necessary to set up the Raspberry Pi 3, installing the Raspbian operating system. This is carried out with the help of a NOOBS microSD card, an external monitor, an HDMI cable, an external keyboard and mouse and a power adapter. In order to complete the installation, the Raspberry Pi must be updated.

The external battery must be charged with a power adapter and connected to the Waveshare 7-inch LCD touchscreen backpack and the Raspberry Pi with two micro-USB cables. The LCD has to be connected using an HDMI cable and by properly configuring the Raspberry Pi's to match the LCD. An optional but practical step is the activation of the VCN graphical system as it allows remote control of the desktop interface of the Raspberry from another computer.

After that, it is necessary to set up the connection of the NoIR camera board by enabling the Raspberry Pi interface. In addition, the dual LED SMT47W/850D is taped paraxially to the camera lens and each of the three terminals are soldered to individual jumper cables. The top right terminal is the common anode and can be connected to a 3.3V GPIO pin on the Raspberry Pi (Pin 1). The bottom left terminal controls the white light and can be connected to GPIO pin 16. The bottom right terminal controls the infrared light, which is connected to a 100-Ohm resistor and then to a GPIO pin 15. Then, one side of the switch button is connected to the ground GPIO pin 6, and the other side to GPIO pin 17. This switch button will act as the shutter button. The electronic design can be seen in figure 23.
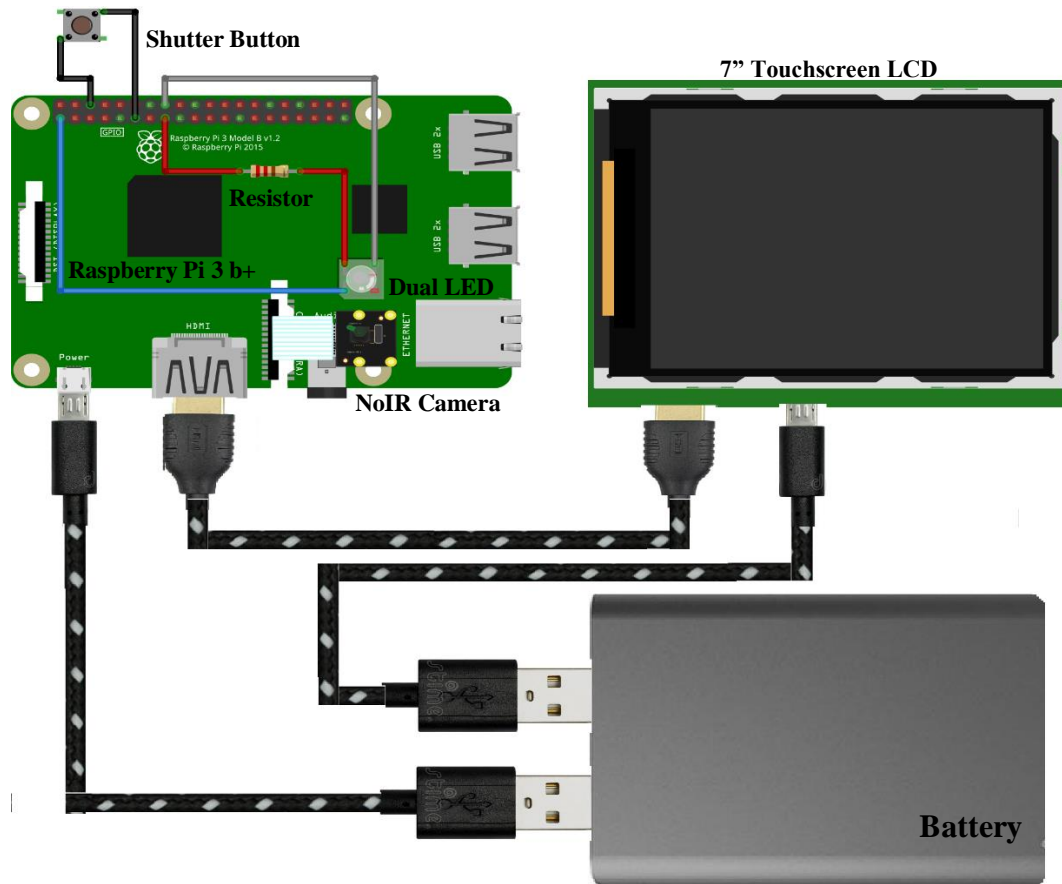
Figure 23. Electronic design of the hardware

When all the components are connected and configured, a script (Annex 1) is written in Python 3 IDLE and then saved on the Raspberry Pi System. This is the non-mydriatic fundus camera program. It will save a picture called "image1" on the desktop when the shutter button is pressed (Figure 24).
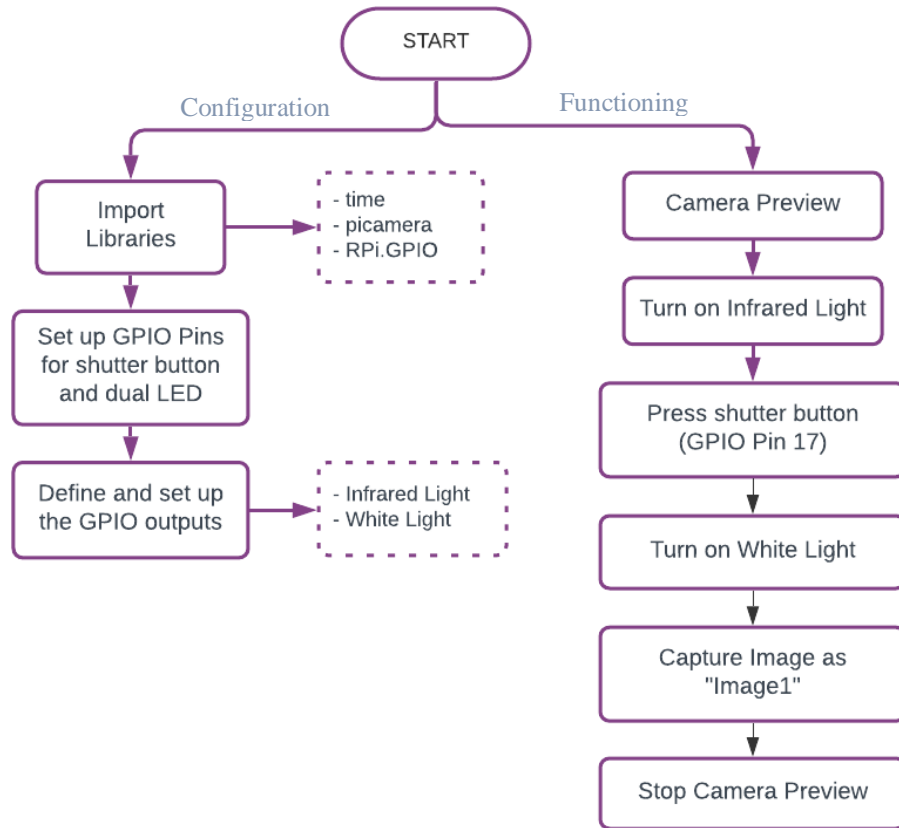
Figure 24. Software for non-mydriatic fundus camera

With all the above described designs, double-sided tape was used to hold all the electronic components together and make it portable. To operate the camera, it is only necessary to plug the micro-USB cable into the Raspberry Pi power port to turn on it. The Raspberry Pi boots up directly onto the desktop. The LCD touchscreen has to be used to open a command window and enter "sudo idle &" into the command window, which will open the Python 3 IDLE program to run the non-mydriatic fundus camera program.

4.2. Software of image processing and pathology detection

For the development of the software, an exploratory investigation on the different methodologies used for digital image processing and analysis was carried out. Also, convolutional neural networks for the classification of diabetic retinopathy according to the presence or absence of symptoms were analyzed.

The development of the models used for processing and analysis of digital images was carried out in MATLAB, a mathematical software that offers an integrated development environment with its own programming language (85). It permits an easy manipulation of matrices, representation of data and functions, implementation of algorithms, and use of toolboxes (85). The Image Processing Toolbox provides a complete set of reference standard algorithms for image processing, analysis and visualization, as well as tools for segmentation, enhancement, noise reduction, geometric transformations, registrations and 3D processing (86).

For the development of our project, MATLAB R2017b was used. Among its advantages are that it provides a comfortable and interactive way to manipulate an image sequence, workflows for object detection and image segmentation to identify pixel regions, as well as evaluate and visualize the results (87).

4.2.1. Dataset of fundus images from STARE

The fundus images for digital processing and analysis were obtained from STARE, a data set containing the fundus images that focus on the structural analysis of the retina (88). These images are in RGB model and JPG format, with a resolution of 700x605 pixels. The STARE project was conceived in 1975 by Michael Goldman at the University of California, San Diego and currently consists of 406 images (88). Goldman's research refers to a system for automatically diagnosing diseases of the human eye by using information formulated to mimic the findings that an ophthalmologist would observe during a clinical examination (88). Figure 25 shows several examples of retinal images obtained from this data set.

Figure 25. Some examples of STARE Dataset. a) Optic Nerve Atrophy, b) Background Diabetic Retinopathy, c) Hypertensive Retinopathy. Source: (88)

The steps implemented for the development of digital image processing and analysis are described in Figure 26.
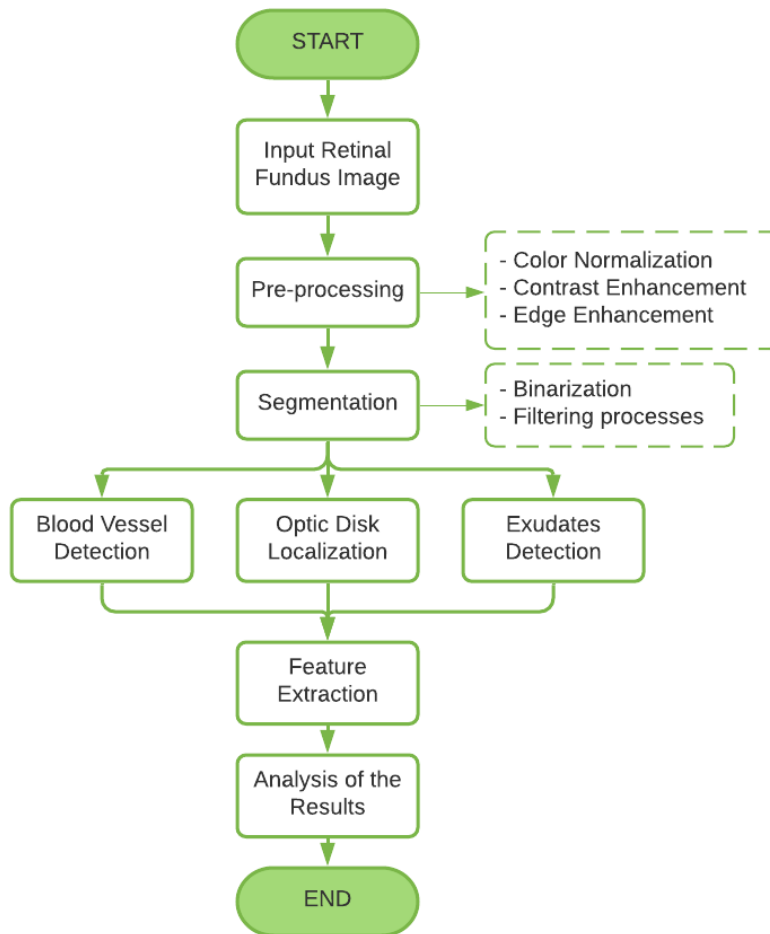
Figure 26. General process for digital image processing and analysis.

The diagram shows the workflow to solve the problem by automatic processing to reveal important findings on a fundus image. The results must be able to show characteristics of the

34

anatomical structures and lesions visible in the image of the retina. This is important to track the severity of the disease and assess the progress of treatment over time.

4.2.2. Preprocessing

This stage is developed with the aim of improving the color normalization, edge enhancement and contrast of the image, highlighting the main characteristics and reducing the portion of the image that are not of interest (89, 90). The present study allows the use of different image preprocessing algorithms as a previous step to segmentation, with the aim of evaluating their impact on the algorithm's performance. An evaluation of the intensity and equalized histograms are used in each component of the RGB model. Contrast enhancement was carried out on the Green component. In addition, morphological operations such as: opening, closing and dilation, erosion were analyzed in order to select the best image option for image pre-processing (Figure 27).
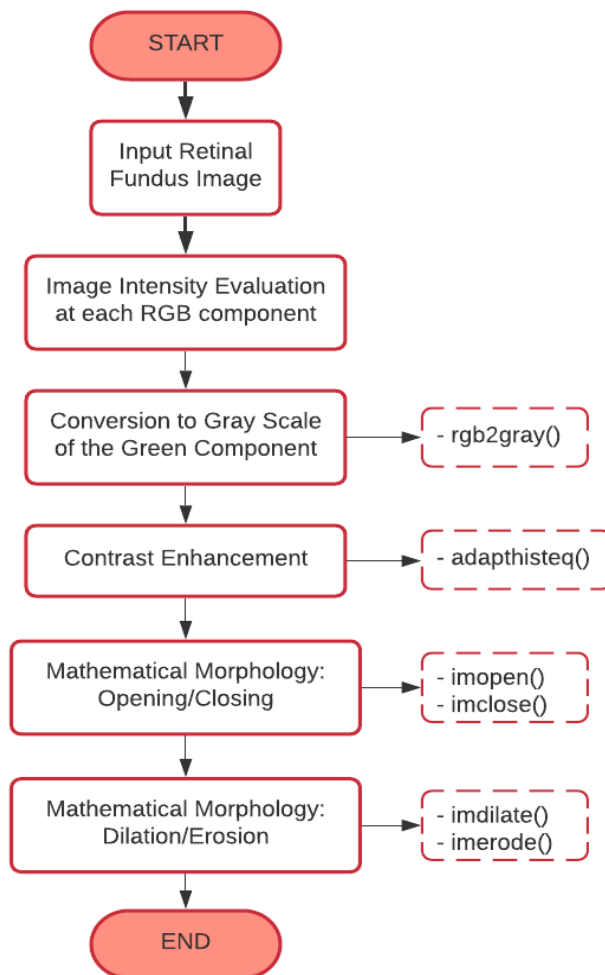
Figure 27. Flow chart for image pre-processing

4.2.3. Segmentation

Image segmentation consists of subdividing the fragments of an image, that is, recognizing and selecting the objects of interest present in an image depending on the problem to be solved (89). In the present project, the segmentation process was used to identify the different parts of interest of the retina, finding variations, reduce noise and detect errors. It was carried out through the use of filtering processes such as Gaussian filter, Laplacian filter and Average filter.
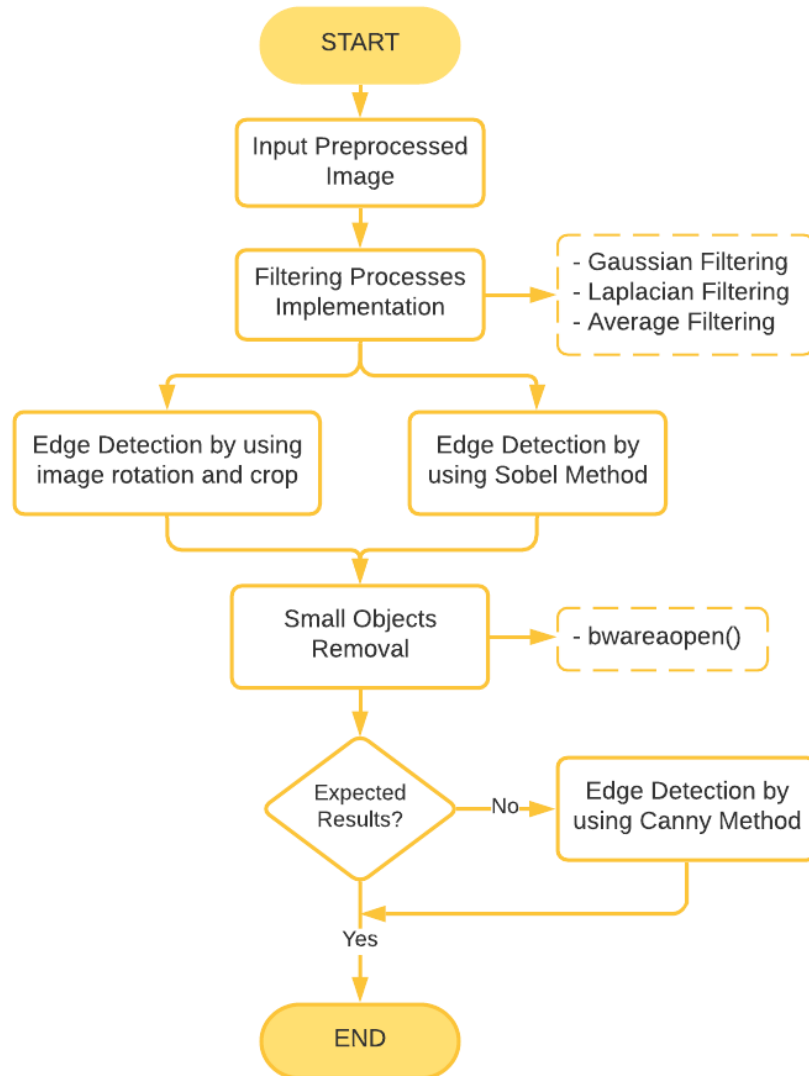
Figure 28. Flow chart for image segmentation.

In addition, the methods used later are based on the analysis of two fundamental properties in an image which are the discontinuity and the similarity (91). Therefore, rotation and crop functions, Sobel and Canny methods were implemented for segmentation in order to achieve edge

and regions detection. Furthermore, it is important to mention that the Sobel method is essential for segmentation but in certain cases, it is not very precise with respect to details and therefore, the Canny method is used as an alternative (Figure 28).

4.2.4. Feature Extraction

The methods for feature extraction are focused on the diagnosis of diabetic retinopathy (92). Certain processes were implemented to provide the algorithm with the ability to differentiate between characteristics of the retina and abnormalities that trigger a type of pathology. Algorithms were carried out to detect, highlight and extract the optic disc, blood vessels and exudates through the use of filtering processes, binary thresholding, mesh grid coordinates, implementation of masks and finally marking the details of interest (Figure 29).
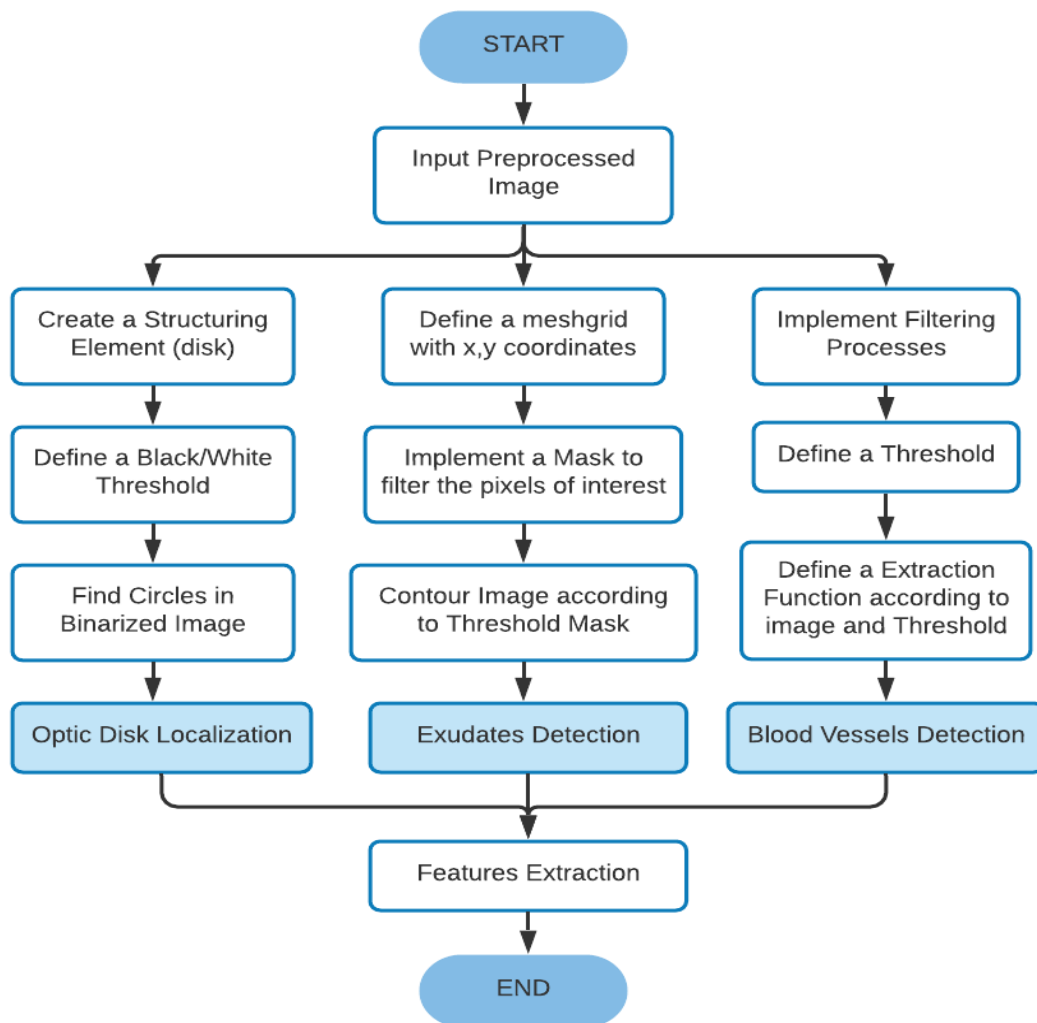
Figure 29. Flow chart for the identification of optic disk, blood vessels and exudates.

4.2.5. Analysis

The analysis consists of the collection of all the procedures previously described in order to design an efficient algorithm able to detect the presence or absence of DR. On one hand, an algorithm focused on image arithmetic operation was implemented. It is a method for the subtraction of an image from another in order to detect the differences between a normal image and an image with retinopathological characteristics (see Figure 30).
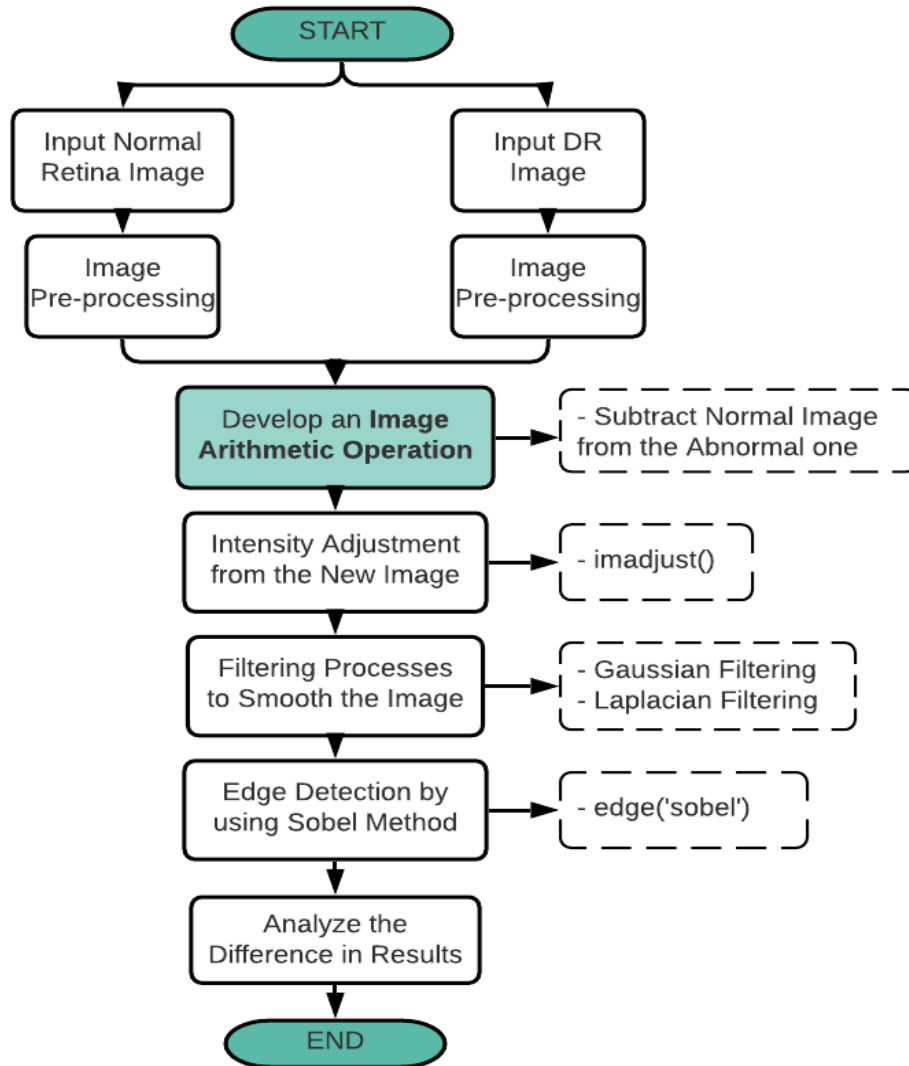
Figure 30. Flow chart for arithmetic algorithm operation.

On the other hand, a software for detecting the number of possible exudates and hemorrhages present in a retinal image was designed. It was carried out detecting the blood vessels and extracting them from the image so that they do not intervene in the analysis. This process allows

isolating the affected areas by this disease, analyze the number of possible anomalies and depending of this, determine the presence or absence of diabetic retinopathy (Figure 31).
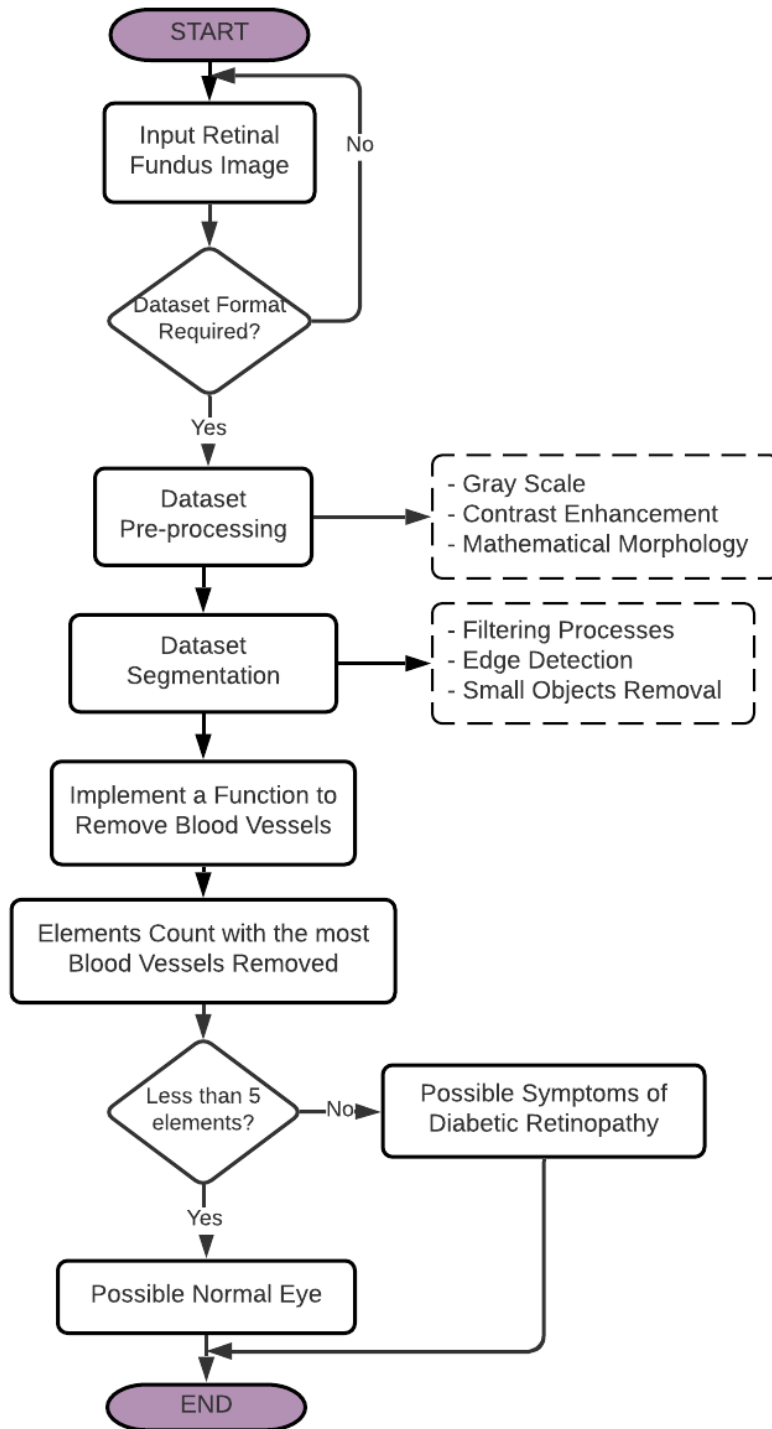
Figure 31. Flow chart for determine diabetic retinopathy presence of absence.

4.3. Convolutional Neural Network

The development of convolutional neural network model was carried out in Python 3.7.0. This is an interpretive programming language that offers many benefits, positioning it as the most widely used language for deep learning (93). Among the main benefits are: its ease of construction of analysis tools, its versatility and availability of numerous packages for neural networks (94).

For the present project we use PyCharm, one of the most complete development environments for Python. It is an application that provides comprehensive services when developing a code in a simpler and more didactic way (95). In order to make the code work properly, it is necessary to install multiple libraries for machine learning, such as: NumPy, Scikit-Learn, TensorFlow, Keras and OpenCV.

- **NumPy:** Provides a data structure that enables the analysis and exchange of data between different algorithms. The data structure implements multidimensional vectors and large capacity matrices (96).
- **Scikit-Learn:** Is a library for data analysis whose advantage lies in the design of classification, regression and grouping algorithms (97).
- **TensorFlow:** Allows to perform numerical calculations using data flow diagrams. It allows for the management of deep neural networks, language processing and image recognition (98).
- **Keras:** Is a high-level interface to work with neural networks, and it is compatible and accessible with TensorFlow. It offers several components related to neuronal layers, activation functions, Pooling, among others (98).
- **OpenCV:** Is a library of open source artificial vision, image analysis and deep learning. It is currently the largest computer vision library in terms of functions and algorithms owned (99).

4.3.1. Dataset of images

The images required for the development of the convolutional neural network model were obtained from Kaggle Platform, an online community of data scientists and machine learning practitioners. This platform launched a competition to identify the signs of diabetic retinopathy in images of the eye, motivated by the need for a comprehensive and automated detection method

using image classification and recognition of patterns (100). The images are in RGB model, type PNG. Also, they have a different size and may vary depending on the identified problem. This happens since the images are captured from different devices (100). Here are typical examples of diabetic retinopathy (Figure 32).
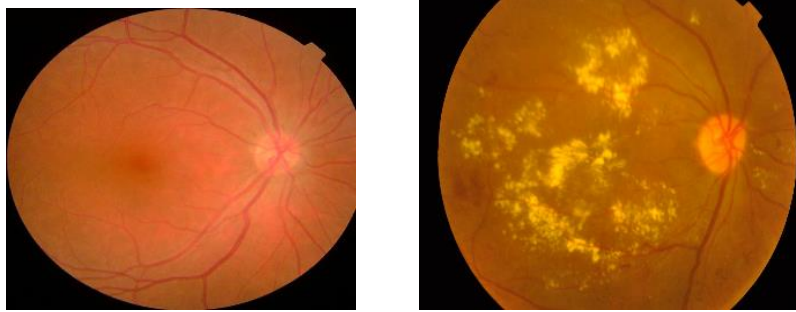
Figure 32. Some examples of Kaggle dataset. a) No Symptoms of Diabetic Retinopathy, b) Symptoms of Diabetic Retinopathy. Source: (100)

The total number of images obtained was 2063, belonging to typical symptoms of diabetic retinopathy. These were divided as follows: 1468 with no symptoms of diabetic retinopathy and 595 with symptoms of diabetic retinopathy. The number of images for each class is unbalanced, for this reason, a randomly chosen fraction of the images was considered to feed the training, validation and evaluation, in a balanced way. The number of images considered can be seen in the Table 5 below.

Table 5. Original Dataset vs. Considered Dataset for CNN

DR Considerations	Original Number	Considered Number
No Symptoms	1468	580
Symptoms	595	580

With the images already selected, the convolutional neural network model was implemented in two different stages. First, a pre-processing stage to improve image quality and contrast, since it is necessary to visualize the blood vessels and optic disc, and to identify the presence of anomalies in as much detail as possible. In addition, the size of each image was resized to develop a more stable model, and thus reduce variability in the samples provided by the data set.

Second, the convolutional neural network model was chosen, among other, for its ability to recognize images. Its architecture allows for the identification and extraction of different characteristics at each stage of diabetic retinopathy required in the classification process and its subsequent automatic diagnosis (101). The procedure is described in Figure 33.
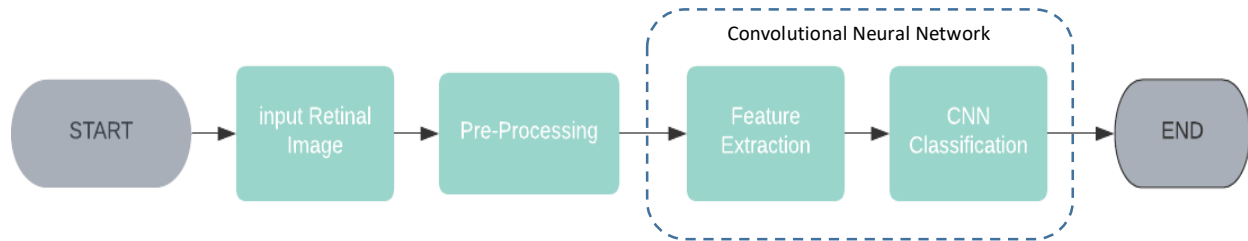
Figure 33. Process for Image Classification.

4.3.2. Preprocessing for CNN

As mentioned above, the data set obtained from the Kaggle Platform offers images of different types of model, size and quality. For this reason, a contrast enhancement and noise reduction methods were implemented by using OpenCV library. It was used cv2.imread to load the image, cv2.bilateralFilter or normalize and finally cv2.resize commands to set the dimensions of the images to 300x300 pixels.

4.3.3. Feature Extraction for CNN

The feature extraction process using convolutional neural networks is a procedure already established by this model, where the network is able to identify the details of each image and later classify them for a pre-diagnosis.

4.3.4. Overall Architecture

The architecture used for the construction of the convolutional neural network was developed following tutorials, references and repositories (102,103) of topics related to the current project. These models were modified depending on our requirements.

Figure 34 shows a graphical representation of the architecture used. The development of several 3x3 convolutional filters can be observed, starting from 32, 64 and 128 feature maps. Following this definition, 2x2 Max Pooling Layer was implemented after each filter. Then, a

flatten filter was included to convert the feature map into a single column that passes to the fully connected layer with 256 neurons, by activating ReLu.
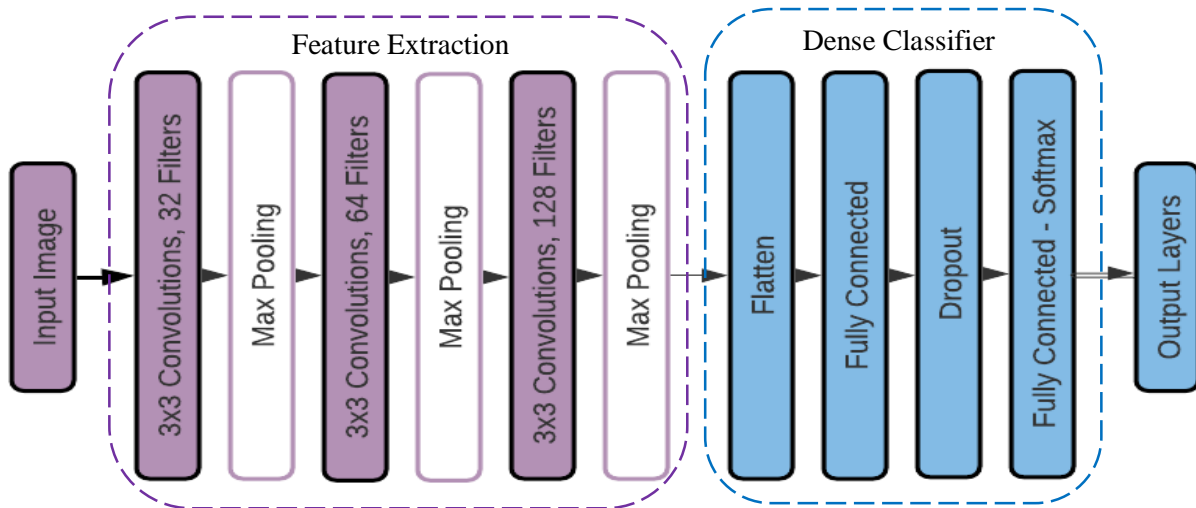
Figure 34. Architecture at each layer of Convolutional Neural Network

Later, a dropout command was implemented with a probability of 0.5, to finally obtain a completely connected layer of two neurons corresponding to the number of classes used in this architecture for subsequent classification using Softmax activation.

4.3.5. Training, Validation, and Testing in CNN

The total number of selected images (1160) was divided in the same way for each class of the diabetic retinopathy (580), depending on the training, validation and evaluation stage. For the development of the training stage, 406 images were considered, corresponding to 70% of the total. On the other hand, for the validation stage, 87 images corresponding to 15% were used and finally, for the evaluation stage, 87 images were selected, the remaining 15%. As it can be seen, the number of images is balanced.

The data set used for the training process is important for each study to aid in the generalization of the model, and in addition to allow for the adjustment of the model parameters. The main characteristic of the training was presenting the neural network what the images look like in each class of diabetic retinopathy, which is used to predict the response of the observations (104). On the other hand, data validation provides an unbiased evaluation of the fit model and is used for

early detection regularization; that is, training has to be stopped when a sign of overfitting to the data is observed. This can be measured, according to metrics like loss and accuracy. Finally, the data set used for the evaluation provided examples to evaluate the performance of the classifier (104).

4.3.6. CNN Model Performance

For the evaluation of the convolutional neural network model, some analysis methods such as validation graphs for accuracy and loss and confusion matrix for the model were used.

- **Validation Graphs**

The validation graphs were created from the history collected during the training process, where the data set is labeled as a test by convention for the model. From the precision graph, it is possible detect the possibility for the model to be further evaluated without showing an overfitting or underfitting of results (105). With the loss graph you can observe the performance of the model, suggesting that the model constantly deviates. When this occurs, it represents a warning sign to stop training in earlier times (105).

- **Confusion Matrix**

Confusion matrix is one of the most intuitive and simple metrics since it allows summarizing the performance of the classification algorithm (64). The parameters evaluated from confusion matrix are accuracy, error rate, sensitivity, specificity and precision. Furthermore, the Kappa Coefficient was evaluated in order to know the concordance between variables and accuracy in the classification (66).

CHAPTER 5

5. RESULTS AND DISCUSION

In chapter six the results obtained with respect to the development of Hardware and Software will be described. First, the operation of the non-mydriatic camera prototype for the acquisition of an image of the fundus is described. Then, the development of the Software is described focusing on two different models. The first describes the processing and analysis of digital images as a search system for the different anomalies that affect the back of the eye: exudates, microaneurysms, hemorrhages, among others. For this, a background diabetic retinopathy image from the STARE database was taken into consideration. The second model focuses on the use of neural networks to classify a retinal image between a normal eye and an eye with diabetic retinopathy using Kaggle dataset.

5.1. Camera Hardware for Retina Detection

5.1.1. Non-mydriatic camera prototype

The non-mydriatic camera prototype can be seen in Figures 35 and 36. The camera measures approximately 100mm x 165mm x 55mm (excluding the size of cables) and weighs approximately 400 grams.

5.1.2. NoIR Camera Function

The operation of the infrared camera module V2 (pi NoIR) yielded successful results at the time of its evaluation, because it offered the ability to visualize in the dark due to its infrared illumination. Figure 37 shows the resolution used by the camera during the dark work environment.
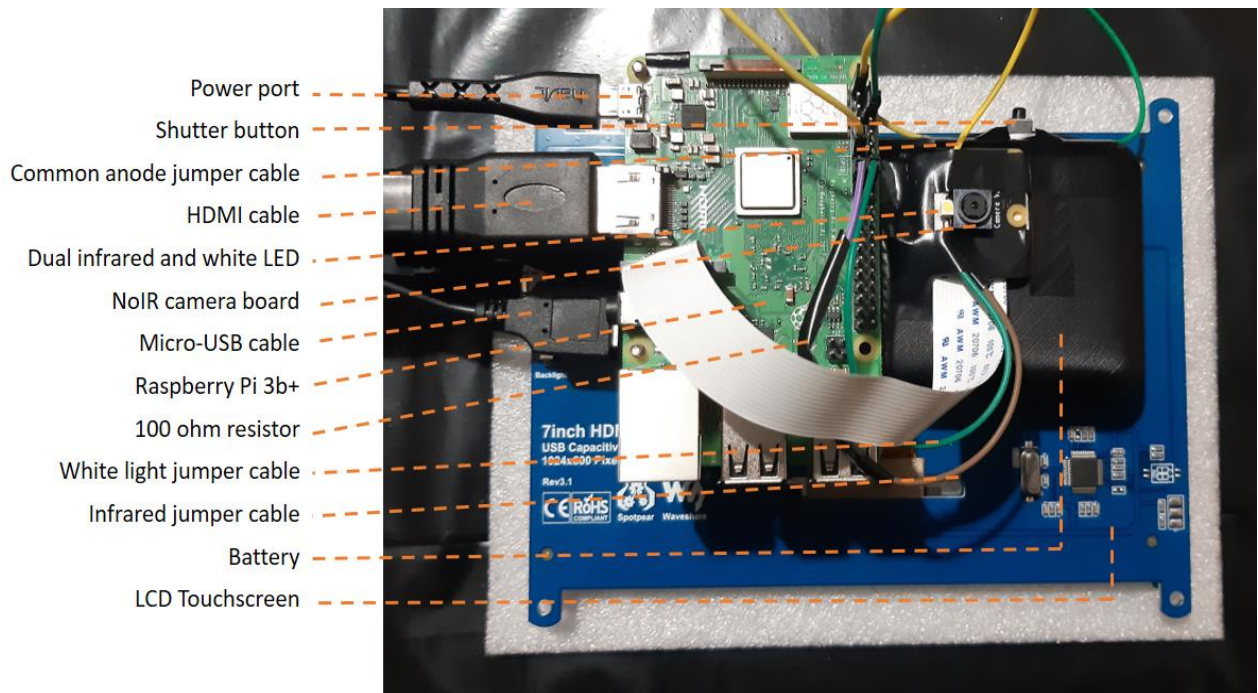
Figure 35. Back part of the camera and used components.
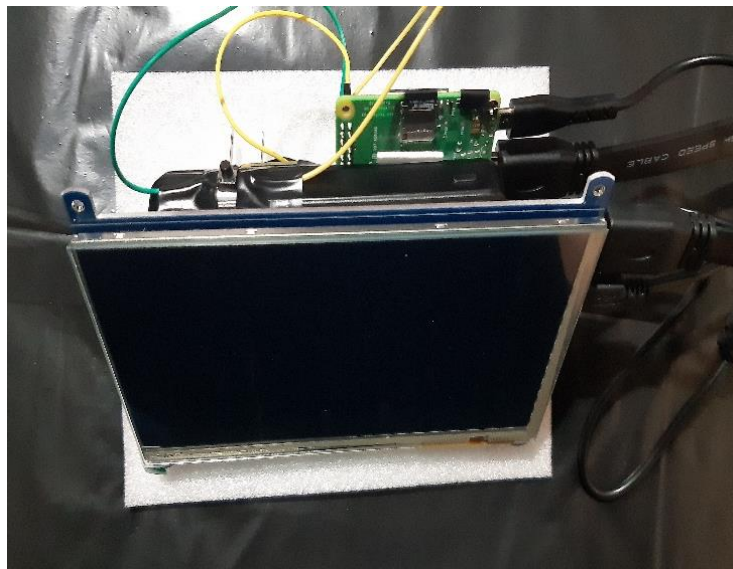
Figure 36. Frontal view of the camera.

Figure 37. Functioning of the Infrared light.

5.1.3. LED SMT47W/850D Function

During the implementation of the working algorithm for image capture, the efficiency of the LED in its two stages could be observed. First, the infrared light is kept on constantly when testing in the dark environment. Second, when the shutter button is pressed, the white light turns on coaxially to briefly illuminate the eye and capture the image (Figure 38).
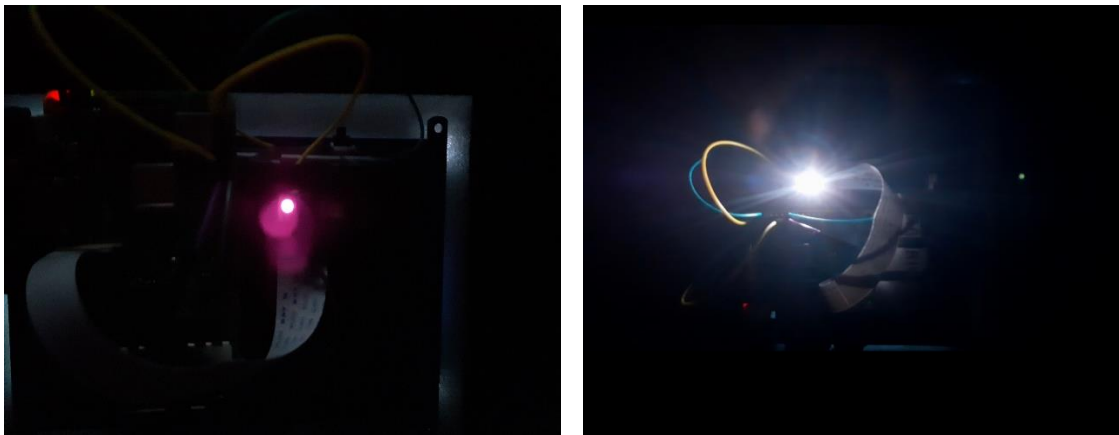
Figure 38: Infrared illumination (Left) and White light illumination (Right).

5.1.4. Camera Function

The non-mydriatic fundus camera is turned on by connecting the micro-USB cable terminal from the 10000mAh battery to the Raspberry pi 3b +. Since the Raspbian operating system has already been installed and configured, the program starts on the desktop. At this time, the

SMT47W/850D LED reflects a soft white and infrared light, ensuring its functionality. Subsequently, the Python 3 IDLE is loaded using "sudo idle & code", at the Raspberry terminal. This allows the camera's viewfinder and infrared LED light to turn on to start the evaluation, as can be seen in the Figure 39.

Figure 39. Functioning of the camera with Infrared light.

For the first performance evaluations, the workplace was set, darkening the room to allow the person's pupils to dilate naturally. The procedure used for the evaluation of indirect ophthalmoscopy through infrared consisted of holding the camera in one hand and the condensing lens in the other, in order to improve focus and image acquisition. This is similar to the mydriatic fundus photography technique using a smartphone.

When the fundus camera, condensing lens, retina, and the patient's pupil are properly aligned, a black and white image can be viewed through the lens viewfinder. When the desired image is displayed, the shutter button is pressed, which immediately turns off the infrared light of the LED and turns on the white light for a very short period of time (500 milliseconds), as a blink.

The evaluation of results focused on selecting fundus images of a person in good quality and focus. The results are satisfactory, but can be improved. Figure 40 (left-hand panel) shows the magnification of the pupil using a 20-diopter ophthalmoscopy lens, while Figure 40 (right-hand panel) shows a section of the retina at the time of capture.
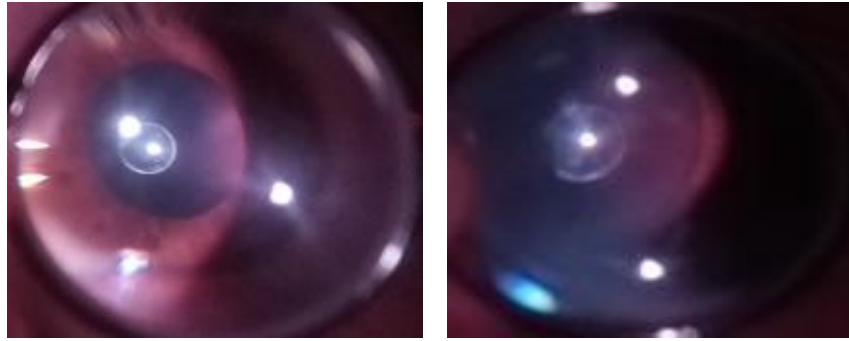
Figure 40. Results from non-mydriatic camera prototype. Left image shows the magnification of the pupil with infrared light when the position of the camera and lens is direct. Right image shows a fragment of the retina captured by the camera in white light illumination.

Finally, the image on the memory card can be accessed and transmitted to a computer via an Ethernet cable or via a download application.

In an investigation conducted by Shen & Mukai, the authors mentioned that the utility of a non-mydriatic camera depends on the distance that can be exerted between a patient's eye, the ophthalmoscopy lens and the camera. At this point, the use of a 20 diopter Volk indirect ophthalmoscopy lens is recommended, with the aim of expanding the viewing and focusing range of the camera (77). The results obtained are satisfactory since the fundus images allow a prudent analysis, as shown in the Figure 41.

Figure 41. Results using the same nonmydriatic camera in infrared light illumination (left) and whith light illumination (right) using Volk lens. Source: (77)

5.2. Software of image processing and pathology detection

5.2.1. Preprocessing

Image Intensity Evaluation

The evaluation of the intensity level implemented to each of the elements in the RGB model allow comparing results according to the visibility in characteristics and determine the best option for the subsequent processes.
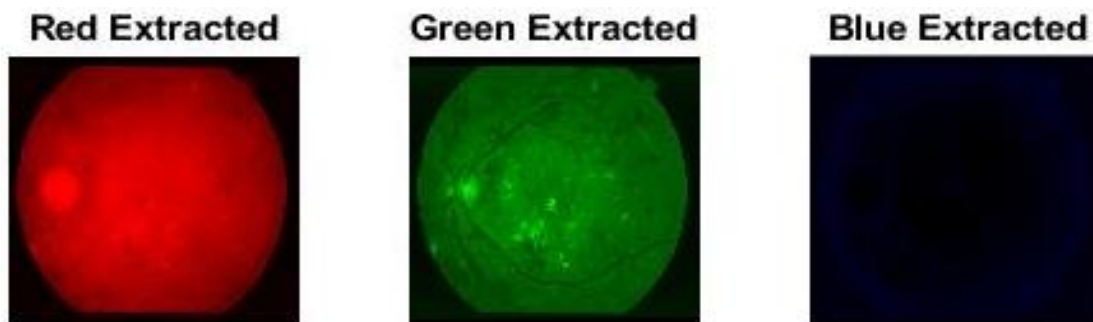
Figure 42. Evaluation of intensity level in red (left), green (middle) and blue (right) components.

In the figure 42, it can be seen how the Green element reflects at a higher level of intensity than Red and Blue elements.
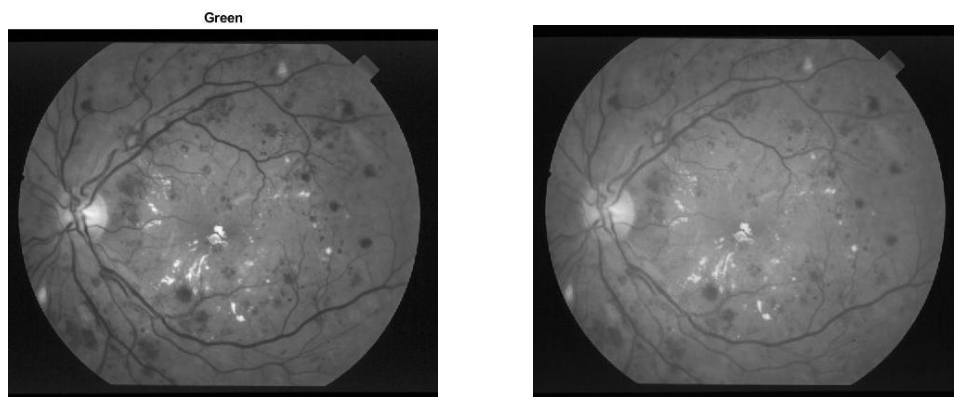
Figure 43. Evaluation of grayscale intensity of Green Component (left) in comparison with Normal Image (right).

Even, comparing the normal model of the image with respect to the Green element, in grayscale, it can be seen how the intensity of the Green element presents an improvement in

contrast, allowing a better identification of the characteristics of the retina such as blood vessels, exudates and optic disc (Figure 43). This is supported by the Figure 44, corresponding to the histogram of each image that suggest that the Green element is the ideal environment for the development of the analysis.
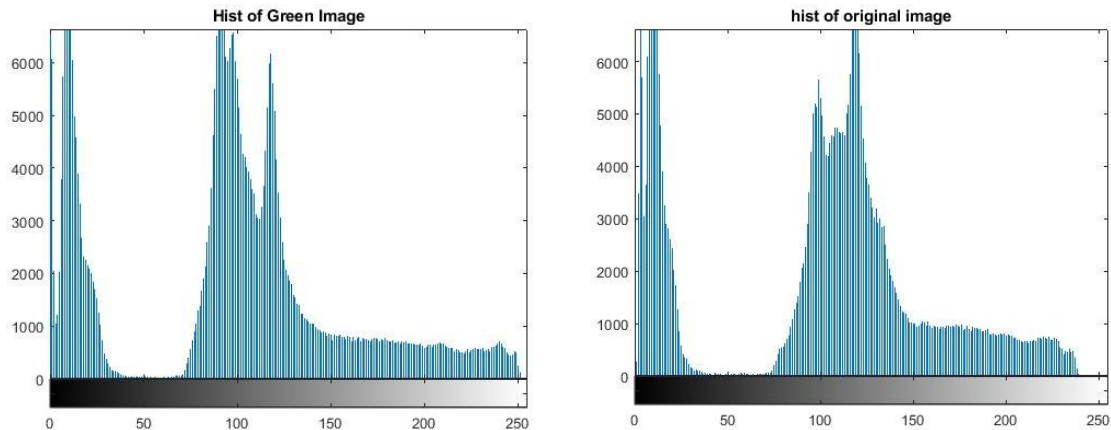
Figure 44. Histograms for intensity evaluation between Green component (left) and Original image (right).

Mathematical Morphology Evaluation

-   **Opening and Closing**

The evaluation carried out between the opening and close operations can be seen in Figure 45. It shows how a morphological operation can visualize a color image in different ways. The opening operation offers a better visualization of the blood vessels in the retina. The closing operation allows better identification of the number of exudates in the retina, while the blood vessels are almost negligible.
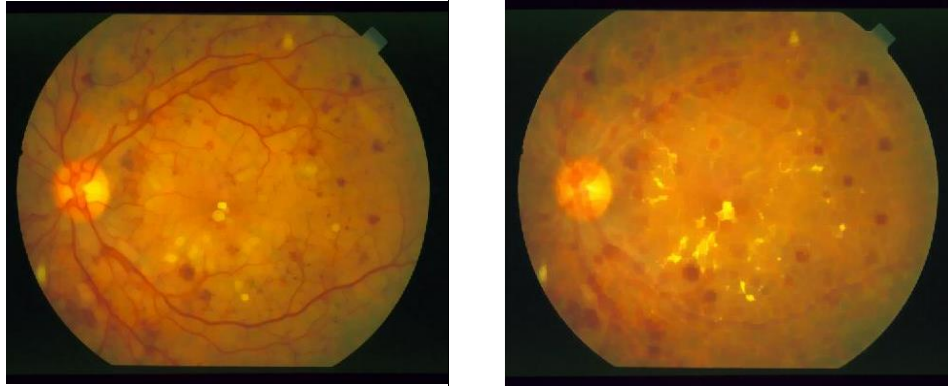
Figure 45. Evaluation of Opening details (left) in comparison with Closing details (right) in color images.

In addition, the same evaluation, corresponding to grayscale images, can be identified in Figure 46. The opening operation shows, in white, the abnormalities present in the retina as a consequence of diabetic retinopathy. In contrast, the close operation does not reflect any evident result, since the dilation process involved in this operation is so great that it does not allow the identification of characteristics.
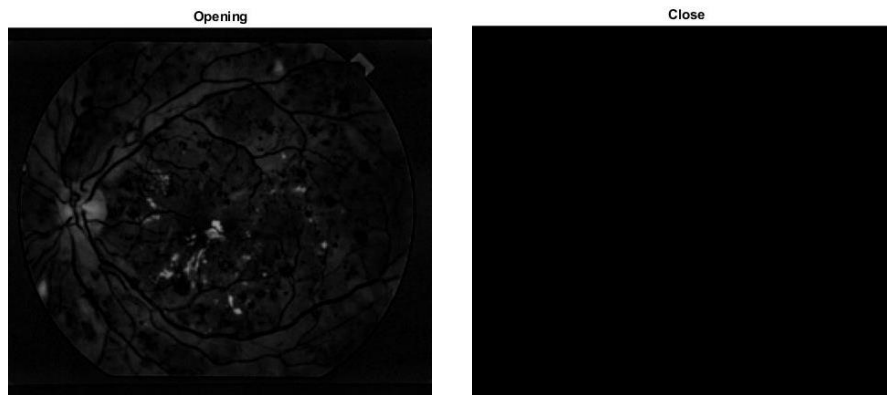
Figure 46: Evaluation of Opening details (left) in comparison with Closing details (right) in grayscale images.

- **Dilation and Erosion**

Figure 47 shows the evaluation corresponding to dilation and erosion of the image. Dilation uses the *disk* function, developing a less marked visualization of the blood vessels, while erosion allows a better visualization of the blood vessels given by the *square* function. It is worth mentioning that these procedures can be carried out with grayscale images.
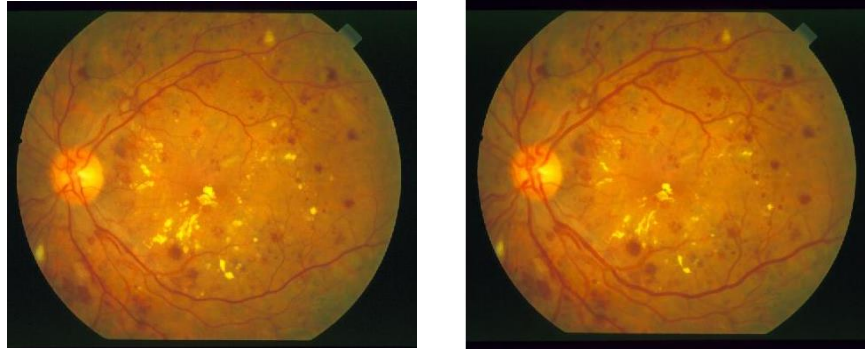
Figure 47. Evaluation of Dilation details (left) in comparison with Erode details (right).

5.2.2. Segmentation

The implemented algorithm for segmentation through filtering procedures, assigning angles for image rotations and their respective morphological crop can be seen in Figure 48. The rotation and crop were performed at the angles of: 0°, 15°, 30°, 45°, 60°, 75°, 90°, 105°, 120°, 135°, 150° and 165°, with the aim of identifying the blood vessels and exudates morphology.
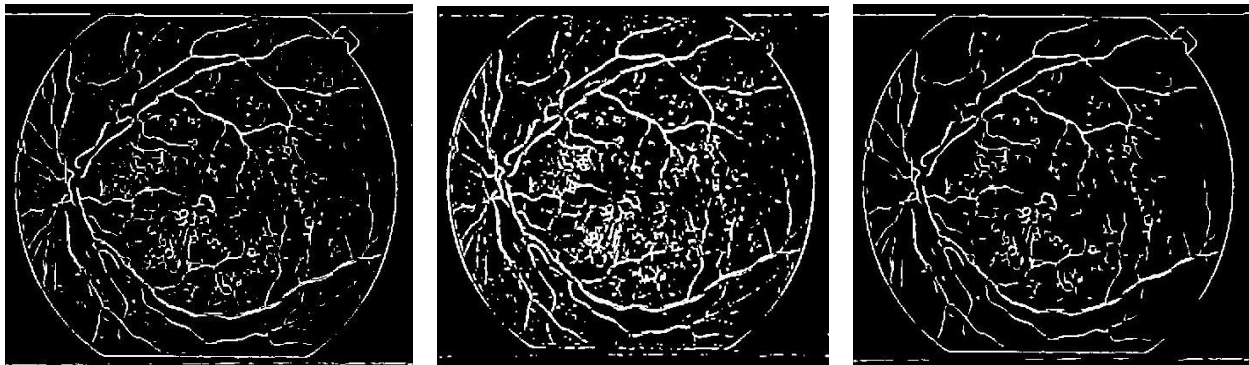
Figure 48. Blood vessels and exudates segmentation with filtering procedures without dilation (left), with dilation (middle) and with small objects removal (right).

In addition, the algorithm focused on Sobel Method for the segmentation of image boundaries and detection of exudates is shown in Figure 49.
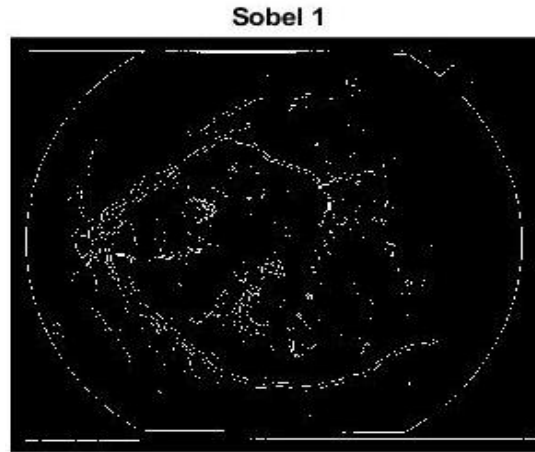
Figure 49. Sobel method for edge detection.

The Sobel method allowed blood vessel identification in a binarized system. It is evident that there are small elements available that do not benefit image analysis. Therefore, they were eliminated on two opportunities through the use of the function *bwareaopen* (Figure 50).
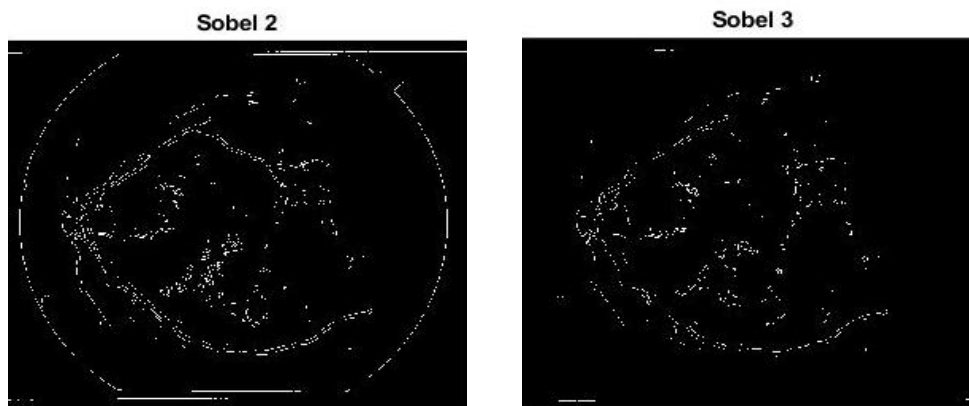
Figure 50. Sobel method with small objects removal. Objects less than 6 pixels (left) and objects less than 6 and more than 40 pixels (right).

However, it can be shown that the small objects removal procedure does not present favorable results, since the detection of important characteristics is almost impossible due to the loss of information.

Therefore, the Canny method was implemented in order to detect blood vessels and exudates of the retina in a more marked way, as can be seen in the Figure 51.
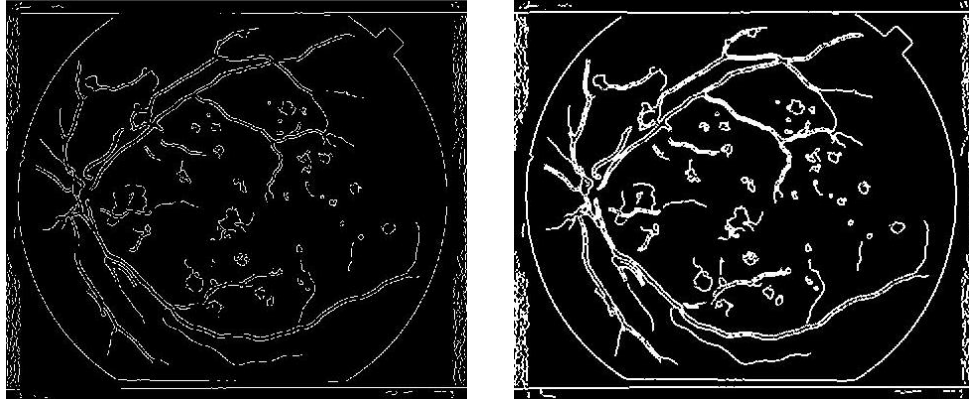
Figure 51. Canny method implementation.

5.2.3. Feature Extraction

Optic Disk Localization

The exact localization of the optic disk in a retina image can be seen in Figure 52. It was achieved through the use of a morphological structuring element *disk* to create a disk-shaped element. The values of thresholding were 160 for white and 12 for black, which allow establishing unequal relationships with the grayscale image.
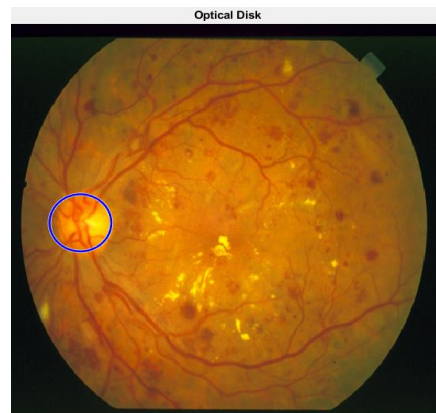
Figure 52. Exact localization of the optic disk

Exudates Localization

The localization of the exudates as a potential feature of diabetic retinopathy was developed through a binary mask model to define the region of interest. The obtained result was defined in the original image using the function *contour*. It can be seen in Figure 53.
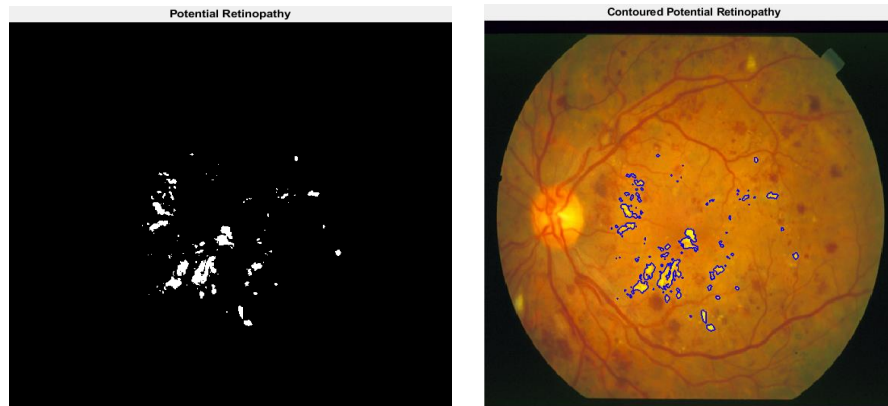
Figure 53. Localization of exudates in binary mask model (left) and contoured in original image (right).

Blood Vessel Localization

The extraction of the blood vessels in a retina image can be observed in Figure 54. It enabled by the functions *metfilt2, median* and *erode,* as a filtering process of the image.
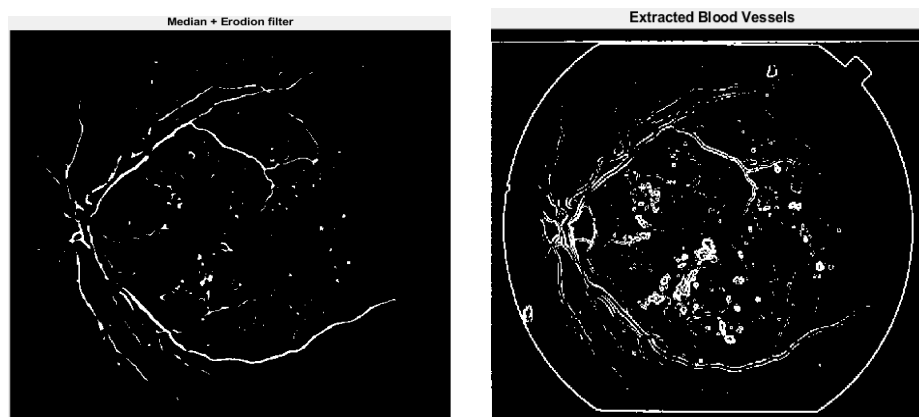
Figure 54. Localization of blood vessels with the use of filters.

5.2.4. Analysis

Image Arithmetic Operation

Figures 55 and 56 show the result of preprocessing to determine the best features of an image with respect to the contrast.
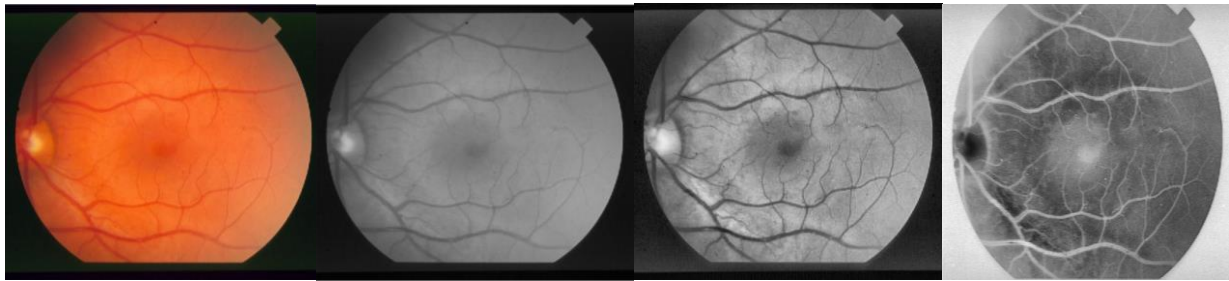
Figure 55. Preprocessing in a normal retina.
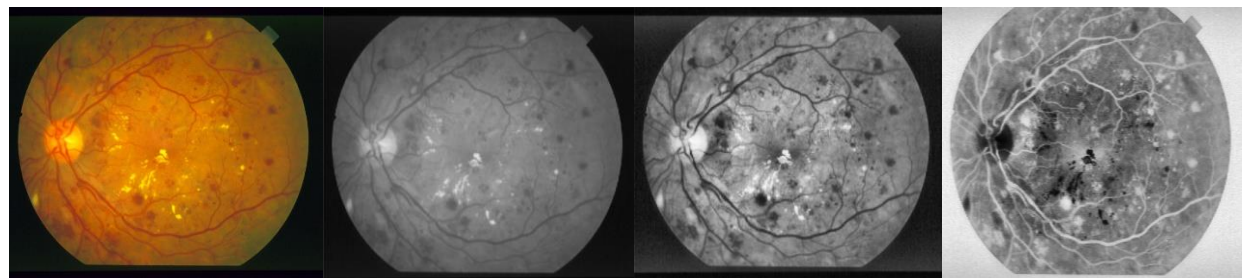
Figure 56. Preprocessing in diabetic retinopathy eye.

In the case of the image corresponding to diabetic retinopathy, the presence of micro-exudates and small hemorrhages can be observed throughout the retina. Therefore, the differences identified regarding the presence or absence of retinal abnormalities during the preprocessing step are evident.

When the process of subtraction is carried out, a new image is obtained where only the affected parts of the retina are marked. This image is subjected to an analysis through the use of Gaussian, filter, Laplacian filter and Sobel method.

An opaque image with the blood vessels and abnormal features can be evidenced with the use of Gaussian and Laplacian filter, while a more detailed image can be observed as the result of Sobel, where the localization of the exudates can be better identified (Figure 57).
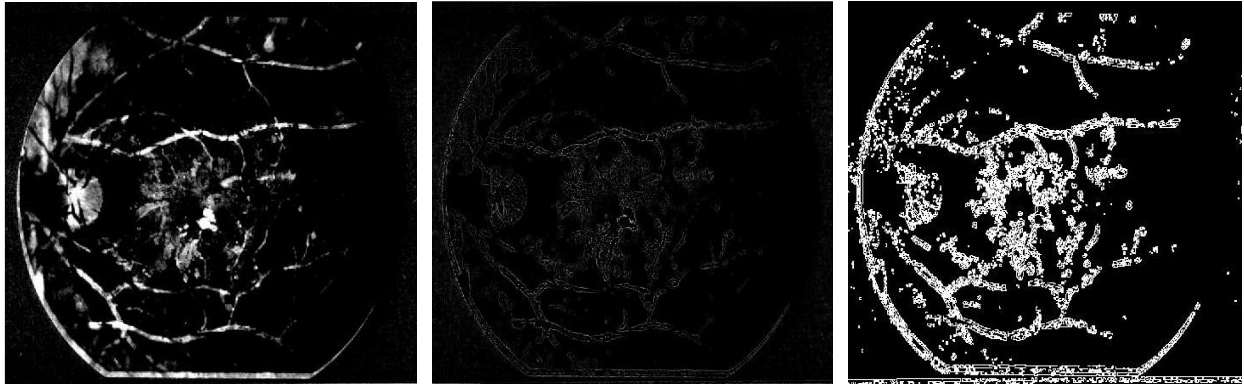
Figure 57. Analysis of results with respect to Gaussian filter (left), Laplacian filter (middle) and Sobel method (right).

Diabetic Retinopathy Detection

Figures 58 and 59 show the features extracted from the images (Normal and DR) that feed the software. This extraction process is necessary to identify possible features of exudates and hemorrhages in the retina and give a pre-diagnosis depending on the results.
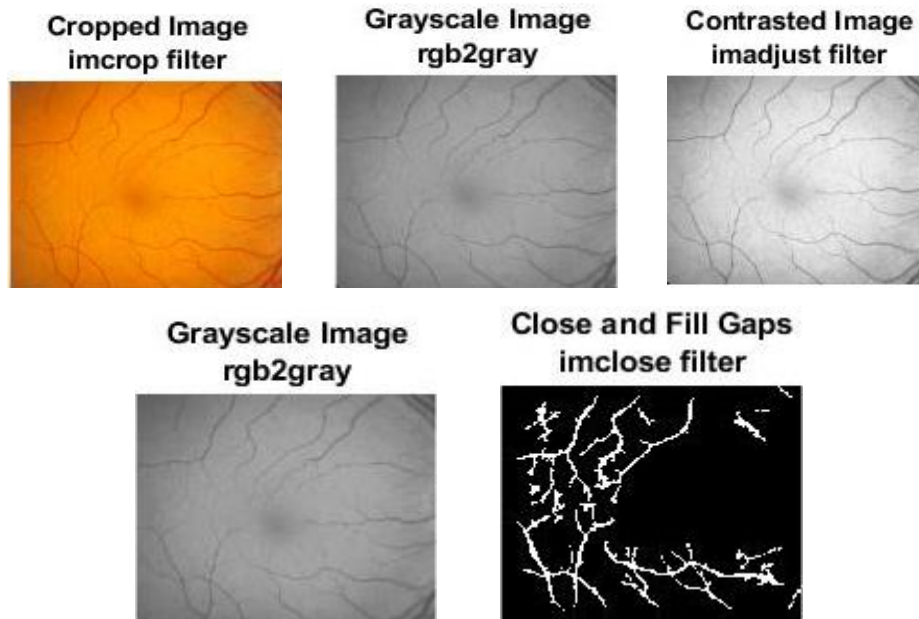
Figure 58. Image features when the pre-diagnosis is a normal retina.
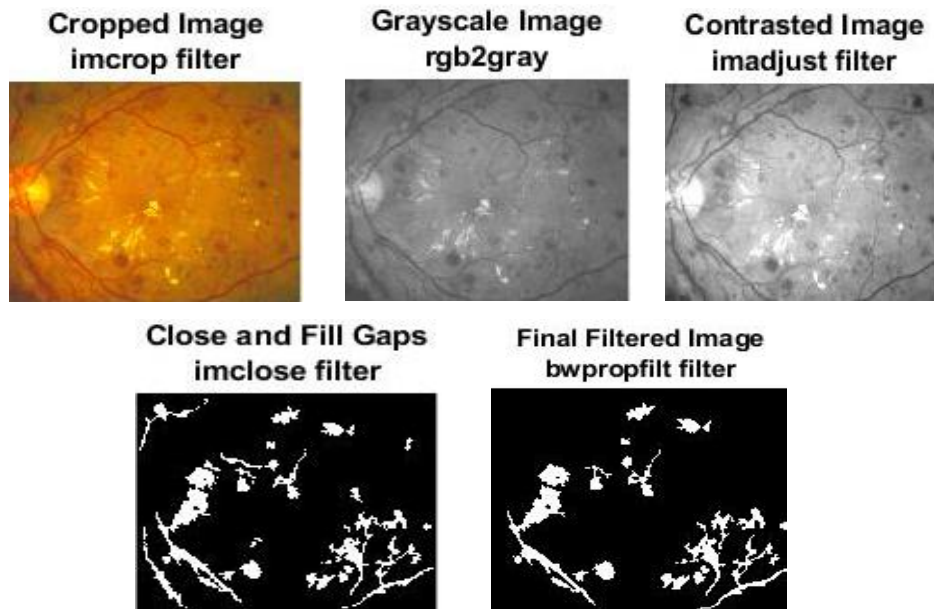
Figure 59. Image features when the pre-diagnosis is DR.

In order to determine the results, the images were subjected to a count of the number of bubbles (exudates and hemorrhages) evidenced during the processing. Figure 60 shows the analysis of 20 images, belonging to the STARE database, to determine the presence or absence of diabetic retinopathy according to the number of hemorrhages identified. The results show that the predictions are correct in the 75% of all cases using a .jpg image format. However, when this format was modified to .ppm, the percentage of correct predictions increased to 80%.

Figure 60. Evaluated images from STARE dataset.

It was concluded that this model guarantees more favorable results depending on the model, format and resolution of the image dataset. Therefore, to determine the significant difference between both formats, a histograms analysis was carried out in order to evaluate the distribution of the pixel values in the images. Figures 61 and 62 show the analysis implemented in both formats. As can be seen, there are small differences in the peaks of the histograms corresponding to each image format, which means that the difference in results, despite being the same image, is due to the change or loss of information in certain sections of the image.
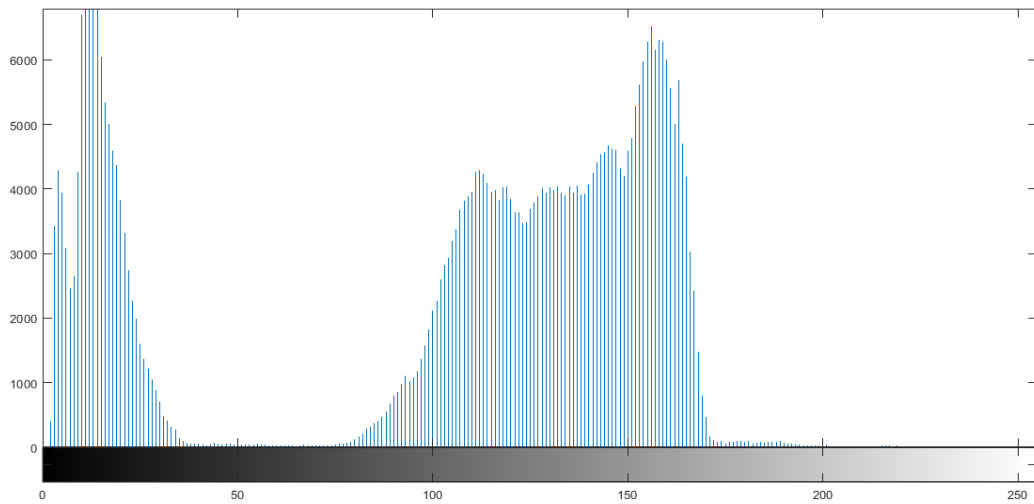
Figure 61. Histogram corresponding to .jpg image format
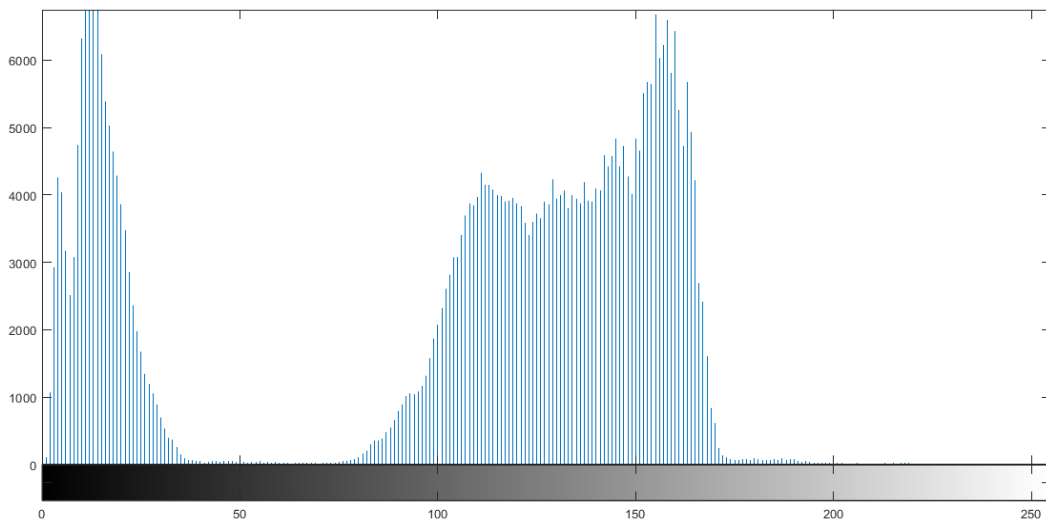
Figure 62. Histogram corresponding to .ppm image format

Furthermore, to obtain quantitative information about histograms, some statistical techniques can be implemented. For example, Asha et al. (106) describe the technique of Chi-square histogram distance as one of the measures of distance used to measure the dissimilarity between two histograms and that is widely used in various applications such as image retrieval and texture, shape and object classification. On the other hand, in a study carried out by Marín (107) two additional techniques, correlation and intersection, are described. Correlation is a bin to bin measure, which refers to a statistical relationship that implies dependence while intersection is a measure of the type bin to bin, which comes from the intersection of the two histograms. All these measures have a high computational performance (107). Therefore, a series of distance measures can be used to compare histograms in various color spaces with various settings of number of bins and number of stripes in the image in order to explain the significant difference that may exist over the image in a dataset.

5.3. Convolutional Neural Network

The proposed model consists of two stages. First, a pre-processing algorithm was developed, in order to improve the image conditions and reduce the number of factors that could affect the convolutional neural network. Second, images obtained from pre-processing enter the network for identification, feature extraction, and classification.

5.3.1. Preprocessing for CNN

The implementation of a pre-processing algorithm should offer the ability to improve image conditions because when working with images of the retina, the difference between a healthy and a diseased eye is minimal. This is why the detection and analysis of exudates and hemorrhages representing a challenge. In the present project, the algorithm used for pre-processing focuses on an improvement in the contrast from the image, allowing identifying the elements present in the retina, such as: blood vessels, optic disk, exudates and hemorrhages (Figure 63).
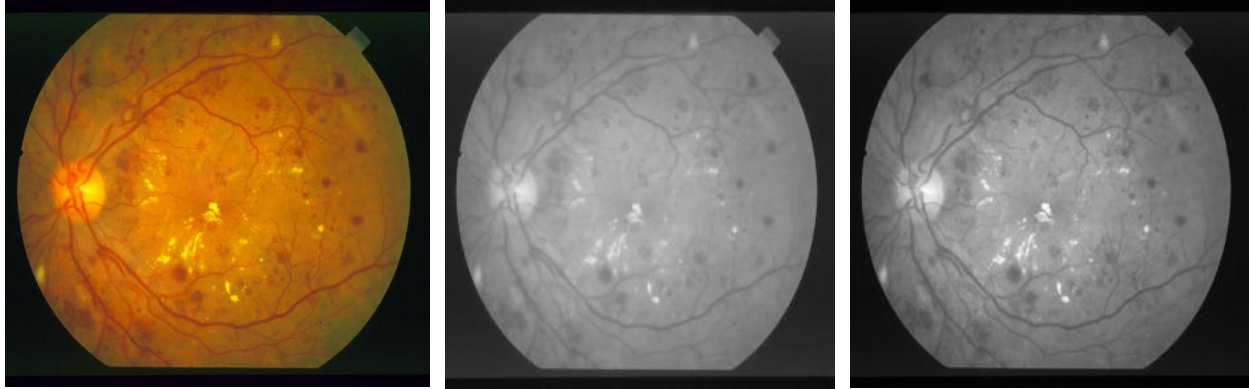
Figure 63. Preprocessing of diabetic retinopathy image (left) with cv2.filter (middle) and normalization (right) for CNN.

Subsequently, the image size was configured to 300x300 pixels, since the images provided by the Kaggle database present varied measurements depending on the device with which they were captured. This allowed feeding the neural network with images of the same size.

5.3.2. CNN Analysis

For the development of a system based on convolutional neural networks, three stages were considered: training, validation and evaluation. The entered data set maintains a balanced structure for the two classes of diabetic retinopathy, where 70% of the images were used for training, 15% for validation and the other 15% for evaluation (Table 6). This structure was carried out to improve the accuracy of the model and thus its validity in solving the problem.

Table 6. Number of images for each class considered in diabetic retinopathy during training, validation and test.

DR Considerations	Training	Validation	Test	TOTAL
No Symptoms	406	87	87	580
Symptoms	406	87	87	580
TOTAL	812	174	174	1160

Several evaluations were carried out in order to determine the parameters necessary for the construction of the neural network, such as batch size, number of epochs, number of steps, convolutional filters and max pooling. Since the present study focuses on a multiclass

classification problem, the model was trained with the use of ReLu activation and Softmax activation, in addition to the categorical cross entropy function (see Annex 2). The chosen parameters for CNN are shown in Table 7.

Table 7. Parameter for Convolutional neural network.

Parameter	Number
Batch Size	32
Epochs	20
Steps	500
Learning Rate	0,0001
Convolutional Filter	3
Max Pooling	3

It can be seen how the neural network is trained through 10000 iterations, using an approximate time of 30 hours. It is worth mentioning that the values chosen for each parameter at the moment of setting the training process have been considered from bibliographic references and model evaluation tests. For example, Pratt et al. use the same learning rate of 0.0001 and 120 epochs in 350 hours of training (101). In contrast, Artola recommends the use of 10 epochs and 32 batch sizes (94). Finally, Shaban et al. describe the training section carried out in 15 epochs (108).

Figures 64 and 65 show the accuracy and loss curves, respectively, for the data set used during training and validation in the final model of the process.

The accuracy function has an increase in each of the 20 epochs, for training and validation. The obtained results in the last epoch are: 0.9903 and 0.6375, respectively. In contrast, the loss function has a decrease in each epoch for training and an increase for validation. In this case the final results are: 0.0313 and 4.3133, respectively.
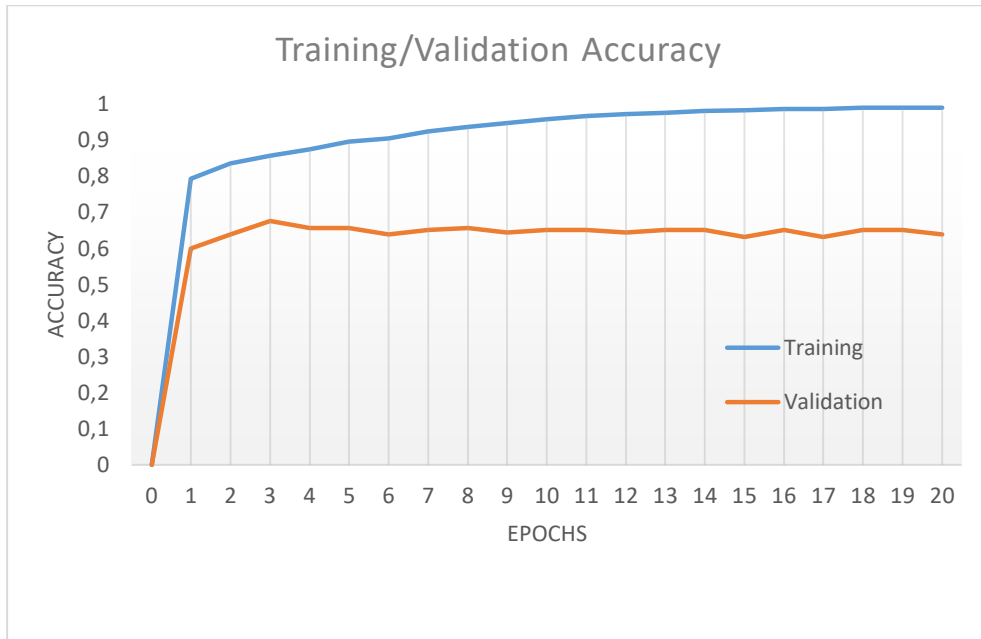
Figure 64. Training/Validation Accuracy. The number of epochs is on the x-axis, while the accuracy value is on the y-axis. In addition, the training curve is shown in blue color and the validation curve is represented by orange color.
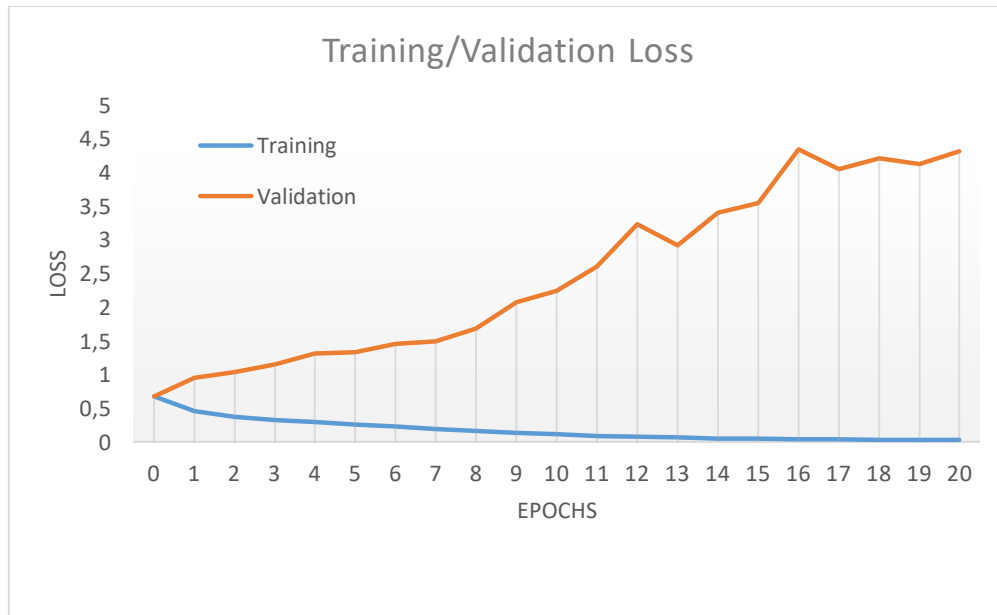
Figure 65. Training/Validation Loss. The number of epochs is on the x-axis, while the loss value is on the y-axis. In addition, the training curve is shown in blue color and the validation curve is represented by orange color.

The results obtained in the figures previously described allow concluding that there is the presence of overfitting in the proposed model. It can be consequence of several factors such as: differences in training and validation data, preprocessing methods used, biased classes, number of epochs among others. The issue of overfitting can be solved by taking some important details into account. For example, the model could be simplified through the removal of objects or number of neurons to make the network smaller and/or using different regularization methods such as: early stopping, use of the data augmentation or the use of dropouts (109). Finally, designing a perfect model is a challenge, because the data set (retina images) is difficult to acquire as it requires a lot of human effort for labeling (110).
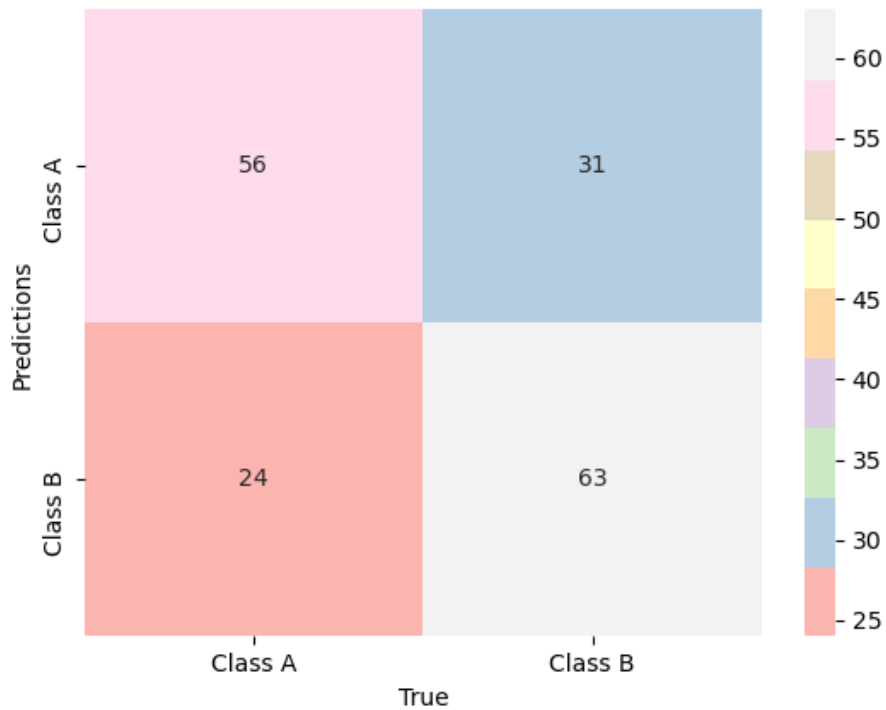
Figure 66. Confusion matrix.

Despite overfitting the obtained results in the testing procedure are good. As is shown in the confusion matrix generated from predictions of the testing dataset (Figure 66), the proposed model can be improved in several ways. For example, in some cases the images with diabetic retinopathy symptoms detected by the neural network did not recognize the patterns consisting of few pixels' characteristic of this pathology and therefore these images were classified as normal.

In order to support these findings, the Table 8 shows the metrics calculated from the confusion matrix. It is important because it can be analyzed, modified and improved for future research works.

Table 8. Metrics calculated from confusion matrix.

Parameter	Value
Accuracy	0,68
Error Rate	0,32
Sensitivity	0,70
Specificity	0,67
Precision	0,64
Kappa Coefficient	0,40

Table 8 shows that the accuracy of the model is 0.68 and the error rate is 0.32. It means that, in the most of the cases, the testing dataset was classified as correct. The sensitivity of the procedure was 0.70, corresponding of the patients correctly identified with DR, specificity is 0.67, corresponding to the patients identified as not having DR and precision of the model is 0.64.

Another accuracy indicator is the Kappa coefficient. It indicates a measure of how the classification results compare to values assigned by chance. The concordance between variables determined by Kappa takes a value of 0.40, which means a fair agreement. This method was considered because of all studies that have sought to evaluate the statistical significance of differences in classification accuracy, many have based the analysis on the comparison of accuracy expressed in terms of the kappa coefficient of agreement (111).

Our results can be compared with those of other investigations in order to determine the efficiency of the algorithm. Table 9 shows the results obtained from two different sources. The first study was carried out by Pratt el al. (101) using a dataset of 80000 retina images, obtaining an accuracy of 0.75, a sensitivity of 0.30 and a specificity of 0.95. On the other hand, Shaban et al. (108) used a dataset of 3648 images to obtain an accuracy and sensitivity of 0.89 and a specificity of 0.95.

Finally, it is important to conclude that the number of images employed in these investigations is very large which can improve the success of a model. Therefore, increasing the data set and processing methods will allow for better results.

Table 9. Proposed model in comparison to other research works.

Source	Dataset	Classes	Accuracy	Sensitivity	Specificity
Pratt et al (101)	80000	5	0.75	0.30	0.95
Shaban et al (108)	3648	5	0.89	0.89	0.95
Proposed Model	1160	2	0.68	0.70	0.67

CHAPTER 6

6. CONCLUSIONS AND RECOMENDATIONS

In the present research work, a prototype of non-mydriatic camera was designed, implemented and evaluated. It functioned properly, correctly allowing visualization and identification of the retina with good resolution. All the bases and principles of functioning were presented so it can be replicated an improved in future work. With respect to the development of software, it is evident that the methods of processing, segmentation, extraction of characteristics and analysis show favorable results in the early diagnosis of diabetic retinopathy because it allows detailed identification of retina abnormalities. In contrast, the convolutional neural network showed an accuracy of 0.68, sensitivity of 0.7, specificity of 0.67 and Kappa Coefficient of 0.40, which represent a highly acceptable statistical significance and agreement between variables.

The development of the prototype of non-mydriatic camera presents considerable results; however, its development could be improved with the implementation of new components. For example, the use of a VOLK lighted indirect ophthalmoscopy lens, which is important for its aspherical structure and much larger diameter to have a larger visible range. In addition, currently a new coaxial LED (SMBB47W / 850D) has been developed, which is much larger and, its functionality for ophthalmoscopy projects has been improved. The multiclass classification method could be improved by taking into account vario0us aspects related to the convolutional neuronal network architecture in order to avoid overfitting and underfitting. For example, one of the most challenging improvements is the acquisition of a well-established dataset that offers excellent image conditions and labeling with the slightest error. This could be achieved by seeking support from hospitals, clinics or health centers that allow expanding the number of retina images to improve the precision, sensitivity and specificity of each stage in a neural network. The mission of the present work is that all people can have access to a pre-diagnostic system in the early stages of the disease so that they can be treated before complications can arise.

REFERENCES

1. Dahl, A. (2020, July 02). Anatomy and Physiology of the Eye. *e Medicine Health.* Retrieved from: https://www.emedicinehealth.com/anatomy_of_the_eye/article_em.htm

2. Garrity, J. (2019, March). Structure and Function of the Eyes. *MSD Manual.* Retrieved from: https://www.msdmanuals.com/home/eye-disorders/biology-of-the-eyes/structure-and-function-of-the-eyes

3. Mittal, K., & Rajam, V. (2020). Computerized retinal image analysis - A survey. *Multimedia Tools and Applications*, 79, 22389-22421. Retrieved from: https://doi.org/10.1007/s11042-020-09041-y

4. Gupta, M., Herzlich, A., Sauer, T. & Chan, C. (2016). Retinal Anatomy and Pathology. *Developments in ophthalmology*, 55(1), 7-17. Retrieved from: https://doi.org/10.1159/000431128

5. *Kolb, H. (2003).* How the Retina Works. *American Scientist,* 91(1), 28-35. *https://doi.org/10.1511/2003.11.841*

6. Golbe, L., Mark, M., & Sage, J. (2007). Parkinson's Disease Handbook. *The American Parkinson Disease Association, Inc.*, 2(3), 69–73.

7. Eye Physician Associates. (2020). Retina. Retrieved from: https://www.eyephysicianassociates.com/comprehensive-eye-care-milwaukee/retina/

8. Kovacs, L., Qureshi, R., Nagy, B., Harangi, B. & Hajdu, A. (2010). Graph Based Detection of Optic Disc and Fovea in Retinal Images. *SOFA 2010—4th International Workshop on Soft Computing Applications, Proceedings*, 7, 143-148. Retrieved from: https://doi.org/10.1109/SOFA.2010.5565610

9. IMAIOS. (2020). Retinal Blood Vessels. Retrieved from: https://www.imaios.com/en/e-Anatomy/Anatomical-Parts/Retinal-blood-vessels

10. Centers for Disease Control and Prevention. (2020, June 3). Common Eye Disorders and Diseases. Retrieved from: https://www.cdc.gov/visionhealth/basics/ced/index.html

11. Medline Plus. (2020, September 16). High blood pressure and eye disease. Retrieved from: https://medlineplus.gov/ency/article/000999.htm

12. Kim, S. (2017, March 31). Making Sense of Hypertensive Retinopathy. *Healthline.* Retrieved from: https://www.healthline.com/health/hypertensive-retinopathy

13. Wu, C., Hu, H., Chou, Y., Huang, N. & Li, C. (2015). High Blood Pressure and All-Cause and Cardiovascular Disease Mortalities in Community-Dwelling Older Adults. *Medicine.* 94(47), 1-10. Retrieved from: https://doi.org/10.1097/MD.0000000000002160

14. Rossi, G., Rossi, A., Sacchetto, A., Pavan, E. & Pessina, A. (1995). Hypertensive Cerebrovascular Disease and Renin-Angiotensin System. *American Heart Organization,* 26(9), 1700-1706. Retrieved from: https://doi.org/10.1161/01.STR.26.9.1700

15. American Heart Association. (2016, October 31). What is High Blood Pressure? Retrieved from: https://www.heart.org/en/health-topics/high-blood-pressure/the-facts-about-high-blood-pressure/what-is-high-blood-pressure

16. Poplin, R., Varadarajan, A., Blumer, K., Liu, Y., McConnell, M., Corrado, G. & Peng, L. (2018). Prediction of cardiovascular risk factors from retinal fundus photographs via deep learning. *Nature Biomedical Engineering.* 2, 158-164. Retrieved from: https://doi.org/10.1038/s41551-018-0195-0

17. National Eye Institute. (2019). La retinopatía Diabética. Retrieved from: https://www.nei.nih.gov/learn-about-eye-health/en-espanol/la-retinopatia-diabetica

18. Aliseda, D. & Berástegui, L. (2008). Diabetic Retinopathy. *Anales del Sistema Sanitario de Navarra,* 31(3), 23-24. Retrieved from: http://scielo.isciii.es/scielo.php?script=sci_arttext&pid=S1137-66272008000600003

19. Eye7. (2020). Diabetic Retinopathy. Retrieved from: https://www.eye7.in/retina/diabetic-retinopathy/

20. Wang, X., Lu, Y., Wang, Y., & Chen, W. (2018). Diabetic Retinopathy Stage Classification Using Convolutional Neural Networks. *IEEE International Conference on Information Reuse and Integration (IRI)*, 465–471. https://doi.org/10.1109/IRI.2018.00074

21. Dubey, S., Jain, K., & Fredrick, T. (2019). Quality assurance in ophthalmic imaging. *Indian Journal of Ophthalmology*, 67(8), 1279-1287. Retrieved from: https://doi.org/10.4103/ijo.IJO_1959_18

22. Bennett, T. & Barry, C. (2009). Ophthalmic imaging today: An ophthalmic photographer's viewpoint - a review. *Clinical & Experimental Ophthalmology*, 37(1), 2-13. Retrieved from: https://doi.org/10.1111/j.1442-9071.2008.01812.x

23. Jin, K., Lu, H., Su, Z., Cheng, C., Ye, J., & Qian, D. (2017). Telemedicine screening of retinal diseases with a handheld portable non-mydriatic fundus camera. *BMC Ophthalmology*, 17(89), 1-7. Retrieved from: https://doi.org/10.1186/s12886-017-0484-5

24. Bennett, T. & Barry, C. (2009). Ophthalmic imaging today: An ophthalmic photographer's viewpoint - a review. *Clinical & Experimental Ophthalmology*, *37*(1), 2-13. Retrieved from: https://doi.org/10.1111/j.1442-9071.2008.01812.x

25. Dubey, S., Jain, K., & Fredrick, T. (2019). Quality assurance in ophthalmic imaging. *Indian Journal of Ophthalmology*, 67(8), 1279-1287. Retrieved from: https://doi.org/10.4103/ijo.IJO_1959_18

26. Navarro, A. (2019). *Desarrollo de un prototipo de cámara de fondo de ojo no midriática.* Tesis de inédita de Maestría en ciencias. Centro de Investigaciones ópticas, Guanajuato, México.

27. International Organization for Standarization (2009, August). ISO 10940:2009 Ophthalmic instruments - Fundus cameras. Retrieved from: https://www.iso.org/standard/39140.html

28. Instituto Ecuatoriano de Normalización. (2014, January). Instrumentos oftálmicos. Cámaras de fondo de ojo (ISO 10940:2009, IDT). Retrieved from: https://www.normalizacion.gob.ec/buzon/normas/nte_inen_iso_10940.pdf

29. Dey, N., Ashour, A. & Borra, S. (2018). *Classification in BioApp. Automation of Decision Making*. Switzerland: Springer International Publishing. Retrieved from: https://doi.org/10.1007/978-3-319-65981-7

30. Ponce, E., Villalobos, F., Damián, P. & Camero, R. (2017). Procesamiento y análisis de imágenes digitales de fondo de ojo para facilitar el telediagnóstico oportuno. *Revista de Cómputo Aplicado,* 1(3), 22-37.

31. Aguirre, N. (2020). *Implementación de un sistema de detección de señales de tráfico mediante visión artificial basado en FPGA.* Tesis inédita de pregrado. Universidad de Sevilla. España.

32. Chavolla, E., Zaldivar, D., Cuevas, E., & Pérez, M. (2018). Color Spaces Advantages and Disadvantages in Image Color Clustering Segmentation. In A. E. Hassanien & D. A. Oliva (Eds.), *Advances in Soft Computing and Machine Learning in Image Processing*, vol. 730, 3–22. Springer International Publishing. https://doi.org/10.1007/978-3-319-63754-9_1

33. Usman, B. & Ayuba, S. (2015). Practical Digital Image Enhancements using Spatial and Frequency Domains Techniques. *International Journal of Computer Science and Software Engineering*, 2(5), 27-32.

34. Mutneja, V. (2015). Methods of Image Edge Detection: A Review. *Journal of Electrical & Electronic Systems*, 04(02), 1-5. Retrieved from: https://doi.org/10.4172/2332-0796.1000150

35. UKEssays. (2018, May 29). Edge Detection Methods in Digital Image Processing. Retrieved from: https://www.ukessays.com/essays/biology/edge-detection-methods-in-digital-image-processing-technology-essay.php?vref=1

36. Said, K. & Jambek, A. (2016). A study on image processing using mathematical morphological. *2016 3rd International Conference on Electronic Design (ICED)*, 507–512. https://doi.org/10.1109/ICED.2016.7804697

37. Hernández, J. (2015). *Procesamiento de imágenes del fondo del ojo para la detección de microaneurismas en la Retinopatía Diabética.* Tesis inédita de pregrado. Instituto Nacional de Astrofísica, Óptica y Electrónica, Puebla, México.

38. Pandey, S., Singh, M. & Pandey, V. (2015). Image Transformation and Compression using Fourier Transformation. *International Journal of Current Engineering and Technology,* 5(2), 1178-1182.

39. Tyagi, V. (2018). *Understanding Digital Image Processing* (1st ed.). Boca Raton: CRC Press. Retrieved from: https://doi.org/10.1201/9781315123905

40. Kumar S., Pathak S., Kumar B. (2019). Automated Detection of Eye Related Diseases Using Digital Image Processing. 513-544. In: Singh A., Mohan A. (eds). *Handbook of Multimedia Information Security: Techniques and Applications*. Springer. https://doi.org/10.1007/978-3-030-15887-3_25

41. Rahim S., Palade V., Jayne C., Holzinger A. & Shuttleworth J. (2015) Detection of Diabetic Retinopathy and Maculopathy in Eye Fundus Images Using Fuzzy Image Processing. (379-388). *Brain Informatics and Health. Lecture Notes in Computer Science*. Springer. https://doi.org/10.1007/978-3-319-23344-4_37

42. Ballabeni, A., Apollonio, F. I., Gaiani, M., & Remondino, F. (2015). Advances in image pre-processing to improve automated 3D reconstruction. *The International Archives of the Photogrammetry, Remote Sensing and Spatial Information Sciences,* 40(5), 315-323.

43. Prakash, R., Saraswathy, G., Ramalakshmi, G., Mangaleswari, K. & Kaviya, T. (2017). Detection of leaf diseases and classification using digital image processing. *International Conference on Innovations in Information, Embedded and Communication Systems,* 1(1), 1–4. Retrieved from: https://doi.org/10.1109/ICIIECS.2017.8275915

44. Maldonado, M. & Eches, E. (2015). *Implementación de Algoritmos para Preprocesamiento, Detección de Bordes y Segmentación de Imágenes Digitales a color utilizando Matlab.* Tesis inédita de pregrado. Universidad Politécnica Nacional, Ecuador.

45. Shashi, P. & Suchithra, R. (2019). Review Study on Digital Image Processing and Segmentation. *American Journal of Computer Science and Technology,* 2(4): 68-72. Retrieved from: http://doi.org/ 10.11648/j.ajcst.20190204.14

46. Yuhen, S. & Hao, Y. (2017). Image Segmentation Algorithms Overview. *Cornell University*, 1(1), 1-6. Retrieved from: https://arxiv.org/abs/1707.02051

47. Claro, M., Santos, L., Lima, W., De Araújo, F., De Moura, N. & Santana, A. (2016). Automatic Glaucoma Detection Based on Optic Disc Segmentation and Texture Feature Extraction. *CLEI Electronic Journal,* 19(2), 1-10. Retrieved from: https://doi.org/10.19153/cleiej.19.2.4

48. Chatterjee, S. (2020, September 24). Feature Extraction in Image Processing. *Great Learning Blog*. Retrieved from: https://www.mygreatlearning.com/blog/feature-extraction-in-image-processing/

49. Nixon, M. & Aguado, A. (2019). *Feature Extraction and Image Processing for Computer Vision.* Southampton: Academic Press. Retrieved from: https://doi.org/10.1016/B978-0-12-814976-8.00001-4.

50. Gavrilova, Y. (2020, April 8). Artificial Intelligence vs. Machine Learning vs. Deep Learning: Essentials. *Serokell.* Retrieved from: https://serokell.io/blog/ai-ml-dl-difference

51. Schmidt, U., Sadeghipour, A., Gerendas, B., Waldstein, S. & Bogunović, H. (2018). Artificial intelligence in retina. *Progress in Retinal and Eye Research*, 67(1), 1–29. Retrieved from: https://doi.org/10.1016/j.preteyeres.2018.07.004

52. Valdez, A. (2018). Introducción al Machine Learning. *Conferencias por el LII Aniversario de la Facultad de Ciencias Puras y Naturales.* Retrieved from: https://doi.org/10.13140/RG.2.2.28886.19527

53. LeCun, Y., Bengio, Y. & Hinton, G. (2015). Deep Learning. *Nature,* 521(1), 436-444. https://doi.org/10.1038/nature14539

54. Kavlakoglu, E. (2020, May 27). AI vs. Machine Learning vs. Deep Learning vs. Neural Networks: What's the Difference? *IBM Cloud Technologies.* Retrieved from: https://www.ibm.com/cloud/blog/ai-vs-machine-learning-vs-deep-learning-vs-neural-networks

55. Mijwel, M., Esen, A. & Shamil, A. (2019). Overview of Neural Networks. *Computer Engineering Techniques Department.* 1, 1-2. Retrieved from: https://www.researchgate.net/publication/332655457_Overview_of_Neural_Networks

56. O'Shea, K., & Nash, R. (2015). An Introduction to Convolutional Neural Networks. *Department of Computer Science,* 1, 1-11. Retrieved from: https://www.researchgate.net/publication/285164623_An_Introduction_to_Convolutional_Neural_Networks

57. Prabhu. (2018, March 4). Understanding of Convolutional Neural Network (CNN) - Deep Learning. *Medium.* Retrieved from: https://medium.com/@RaghavPrabhu/understanding-of-convolutional-neural-network-cnn-deep-learning-99760835f148

58. MissingLink.AI. (2020). Convolutional Neural Network Architecture: Forging Pathways to the Future. Retrieved from: https://missinglink.ai/guides/convolutional-neural-networks/convolutional-neural-network-architecture-forging-pathways-future/

59. Tomar, N. (2020, May 28). What are convolutional layers? *Quora.* Retrieved from: https://www.quora.com/What-are-convolutional-layers

60. Alom, Z., Taha, T., Yakopcic, C., Westberg, S., Sidike, P., Nasrin, M., Hasan, M. & Asari, V. (2019). A State-of-the-Art Survey on Deep Learning Theory and Architectures. *Electronics,* 8(1), 1-67. Retrieved from: https://doi.org/10.3390/electronics8030292

61. Saha, S. (2018, December 15). A Comprehensive Guide to Convolutional Neural Networks - the ELI5 way. *Towards Data Science*. Retrieved from: https://towardsdatascience.com/a-comprehensive-guide-to-convolutional-neural-networks-the-eli5-way-3bd2b1164a53

62. Bhodi, I. (2020, July 2). Overfitting and Underfitting. *Medium.* Retrieved from: https://medium.com/@itbodhi/overfitting-and-underfitting-in-machine-learning-models-76cb60dbdaf6

63. Heidari, J. (2019). *Classifying Material Defects with Convolutional Neural Networks and Image Processing.* Tesis inédita de pregrado. Universidad Uppsala, Suecia.

64. ClassEval. (2020). Basic evaluation measures from the confusion matrix. Retrieved from: https://classeval.wordpress.com/introduction/basic-evaluation-measures/

65. Ukrainski, P. (2016, September 23). Classification Accuracy Assessment. Confusion Matrix Method. *North Spatial.* Retrieved from: http://www.50northspatial.org/classification-accuracy-assessment-confusion-matrix-method/

66. Scarpelli, G. (2020). Cohen's Kappa free calculator. *Ido Statics.* Retrieved from: https://idostatistics.com/cohen-kappa-free-calculator/

67. World Health Organization. (2020). Global report on diabetes. Retrieved from: https://www.who.int/diabetes/global-report/en/

68. Novalab Ibérica. (2020, January 2). Diabetes tipo 1. Retrieved from: https://objetivo-cerohipoglucemias.es/diabetes-tipo1/asi-empieza-el-2020-la-diabetes-en-el-mundo.html

69. World Health Organization. (2020, June 8). Diabetes. Retrieved from: https://www.who.int/news-room/fact-sheets/detail/diabetes

70. The International Agency for the Prevention of Blindness. (2020). Diabetic Retinopathy. Retrieved from: https://www.iapb.org/knowledge/what-is-avoidable-blindness/diabetic-retinopathy/

71. Cheloni, R., Gandolfi, S., Signorelli, C. & Odone, A. (2019). Global prevalence of diabetic retinopathy: Protocol for a systematic review and meta-analysis. *BMJ Open*, *9*(3), 1-5. Retrieved from: https://doi.org/10.1136/bmjopen-2018-022188

72. Organización Panamericana de la Salud. (2020). La diabetes, un problema prioritario de salud pública en el Ecuador y la región de las Américas. Retrieved from: https://www.paho.org/ecu/index.php?option=com_content&view=article&id=1400:la-

diabetes-un-problema-prioritario-de-salud-publica-en-el-ecuador-y-la-region-de-las-americas&Itemid=360

73. Sarrazin, L. (2016, February 9). Retinopatía diabética: tercera causa de ceguera en Ecuador. *Revista Vive.* Retrieved from: https://revistavive.com/retinopatia-diabetica-tercera-causa-de-ceguera-en-ecuador/

74. Flores, K. & Jara, K. (2016). *Factores de riesgo asociados a retinopatía diabética en pacientes con diabetes mellitus tipo 2 entre 30 y 60 años de edad, en el hospital san francisco de quito durante el período de enero del 2013 a enero del 2015.* Tesis inédita de pregrado. Pontificia Universidad Católica del Ecuador.

75. World Health Organization. (2020). Blindness and vision impairment prevention. Retrieved from: https://www.who.int/blindness/causes/priority/en/index5.html

76. Monroy, J. (2018, October 5). Dispositivos médicos, aliados en prevención y tratamiento de enfermedades. *Las 2 Orillas.* Retrieved from: https://www.las2orillas.co/dispositivos-medicos-aliados-en-prevencion-y-tratamiento-de-enfermedades/

77. Shen, B., & Mukai, S. (2017). A Portable, Inexpensive, Nonmydriatic Fundus Camera Based on the Raspberry Pi® Computer. *Journal of Ophthalmology*, vol. 2017, 1-5. Retrieved from: https://doi.org/10.1155/2017/4526243

78. Raspberry Pi Organization. (2020). Raspberry Pi 3 Model B+. Retrieved from: https://static.raspberrypi.org/files/product-briefs/Raspberry-Pi-Model-Bplus-Product-Brief.pdf

79. Educba. (2020). Differences between Raspberry Pi and Arduino. Retrieved from: https://www.educba.com/raspberry-pi-3-vs-arduino/

80. Google Sites. (2020). Nexys 4 Artix-7 FPGA Board. Retrieved from: https://sites.google.com/site/logicaprogramable/calculadoras/fpga/nexys-4-artix-7-fpga-board

81. Raspberry Pi Organization. (2020). Pi NoIR Camera V2. Retrieved from: https://www.raspberrypi.org/products/pi-noir-camera-v2/

82. Marubeni America Corporation. (2020). SMT47W/850D LED. Retrieved from: http://tech-led.com/wp-content/uploads/2017/05/SMT47W-850D.pdf

83. Zizowireless. (2020). HAVIT H584 Portable Power Bank 10,000 mAh. Retrieved from: https://www.zizowireless.com/products/havit-h584-portable-power-bank-10-000-mah

84. Waveshare. (2020). 7inch Capacitive Touch Screen LCD. Retrieved from: https://www.waveshare.com/7inch-hdmi-lcd-c.htm

85. Medrano, B. (2014). Procesamiento de imágenes con MATLAB. *Dpto. Matemática Aplicada 1,* 1, 1-20. Retrieved from: https://personal.us.es/majiro/2014_10_10_clase2.pdf

86. Math Works. (2020). Image Processing Toolbox. Retrieved from: https://es.mathworks.com/products/image.html

87. Natick, M. (2017, September 21). MathWorks News and Stories. *Math Works.* Retrieved from: https://es.mathworks.com/company/newsroom/mathworks-announces-release-2017b-of-the-matlab-and-simulink-product-families.html

88. Cecas Clemson. (2020). STructured Analysis of the Retina (STARE). Retrieved from: https://cecas.clemson.edu/~ahoover/stare/

89. Vásquez, Y., Flórez, M., Beltrán, C. & Gómez, M. (2016). Procesamiento de las Imágenes con Matlab (Venas de los dedos). *Universitaria de Investigación y Desarrollo*, 1, 1-31.

90. Valencia, J., Poveda, D. & Valencia, D. (2014). Evaluación del impacto del preprocesamiento de imágenes en la segmentación del iris. *Tecno Lógicas*, *17*(33), 31-41. Retrieved from: http://www.scielo.org.co/pdf/teclo/v17n33/v17n33a04.pdf

91. Chiriboga, M. & Salcedo, E. (2003). *Implementación de algoritmos para preprocesamiento, detección de bordes y segmentación de imágenes digitales a color utilizando Matlab.* Tesis inédita de pregrado. Escuela Politécnica Nacional, Ecuador.

92. Khan, M. (2013). Diabetic Retinopathy Detection using Image Processing: A Survey. *International Journal of Emerging Technology & Research,* 1(1), 16-20. Retrieved from: https://www.researchgate.net/publication/279530174_Diabetic_Retinopathy_Detection_using_Image_Processing_A_Survey

93. González, R. (2020). Python para todos. Retrieved from: https://www.utic.edu.py/citil/images/Manuales/Python_para_todos.pdf

94. Artola, A. (2019). *Clasificación de imágenes usando redes neuronales convolucionales en Python*. Tesis de pregrado. Universidad de Sevilla, España.

95. Escuela de Python. (2020). Pycharm: uno de los mejores IDE para Python. Retrieved from: https://www.escuelapython.com/pycharm-uno-de-los-mejores-ide-para-python/

96. Martínez, J. (2019). Librerías de Python para Machine Learning. *IArticial.* Retrieved from: https://www.iartificial.net/librerias-de-python-para-machine-learning/

97. Chapaval, N. (2017). Cuatro librerías de Machine Learning: TensorFlow, Scikit-learn, Pytorch y Keras. *Platzi.* Retrieved from: https://platzi.com/blog/librerias-de-machine-learning-tensorflow-scikit-learn-pythorch-y-keras/

98. Costa, C. (2020, March 24). Best Python Libraries for Machine Learning and Deep Learning. *Towards Data Science.* Retrieved from: https://towardsdatascience.com/best-python-libraries-for-machine-learning-and-deep-learning-b0bd40c7e8c

99. Marín, R. (2020, February 12). ¿Qué es OpenCV? Instalación en Python y ejemplos básicos. *Revista Digital INESEM.* Retrieved from: https://revistadigital.inesem.es/informatica-y-tics/opencv/

100. Kaggle. (2020). Diabetic Retinopathy Detection Dataset. Retrieved from: https://www.kaggle.com/c/diabetic-retinopathy-detection/data

101. Pratt, H., Coenen, F., Broadbent, D., Harding, S. & Zheng, Y. (2016). Convolutional Neural Networks for Diabetic Retinopathy. *Procedia Computer Science*, 90(1), 200-2005. Retrieved from: https://doi.org/10.1016/j.procs.2016.07.014

102. Puig, A. (2018, July 19). *Cómo hacer un clasificador de imágenes desde cero con Tensorflow.* [Video File]. Retrieved from: https://www.youtube.com/watch?v=EAqb20_4Rdg

103. Puig, A. (2018). CNN desde cero. *AMP Tech.* Retrieved from: https://github.com/puigalex/AMP-Tech/tree/master/CNN%20desde%20cero

104. Wiki. (2020). Conjuntos de entrenamiento, validación y pruebas - Training, validation, and test sets. Retrieved from: https://es.qwe.wiki/wiki/Training,_validation,_and_test_sets

105. Brownlee, J. (2019, October 3). Display Deep Learning Model Training History in Keras. *Machine Learning Mastery.* Retrieved from: https://machinelearningmastery.com/display-deep-learning-model-training-history-in-keras/

106. Asha, V., Bhajantri, N. & Nagabhushan, P. (2012). GLCM based Chi-square Histogram Distance for Automatic Detection of Defects on Patterned Textures. *Computer Vision and Pattern Recognition,* 2(4), 302-313. Retrieved from: https://doi.org/10.1504/IJCVR.2011.045267

107.   Marín, P. (2015). *Estudio comparativo de medidas de distancia para histogramas en problemas de reidentificación.* Tesis inédita de Maestría. Universidad de las Palmas de Gran Canaria, España.

108.   Shaban, M., Ogur, Z., Mahmoud, A., Switala, A., Shalaby, A., Khalifeh, H., Ghazal, M., Fraiwan, L., Giridharan, G., Sandhu, H. & El-Baz, A. (2020). A convolutional neural network for the screening and staging of diabetic retinopathy. *PLOS ONE*, 15(6), 1-13. Retrieved from: https://doi.org/10.1371/journal.pone.0233514

109.   Sagar, A. (2019). 5 Techniques to Prevent Overfitting in Neural Networks. *KDnuggets News*. Retrieved from: https://www.kdnuggets.com/2019/12/5-techniques-prevent-overfitting-neural-networks.html

110.   Ying, X. (2019). An Overview of Overfitting and its Solutions. *Journal of Physics: Conference Series*, 1168(1), 1-7. Retrieved from: https://doi.org/10.1088/1742-6596/1168/2/022022

111.   Foody, G. (2004). Thematic Map Comparison: Evaluating the Statistical Significance of Differences in Classification Accuracy. *American Society for Photogrammetry and Remote Sensing,* 70(5), 627-633.

ANNEXES

- *Annex 1. Python script to capture the image in non-mydriatic camera*

```python
import time
import picamera
import RPi.GPIO as GPIO

GPIO.setmode(GPIO.BCM)
GPIO.setup(17, GPIO.IN, GPIO.PUD_UP)
# GPIO 17 is the shutter button
GPIO.setup(22, GPIO.OUT)
# GPIO 22 is the infrared cathode
GPIO.setup(23, GPIO.OUT)
# GPIO 23 is the white light cathode
GPIO.output(22, False)
# Sets the infrared cathode to ground.
# Common anode of the LED is set to 3.3 V, so setting GPIO 22 to ground
# causes the infrared light to be on.
GPIO.output(23, True)
# Sets the white light cathode to 3.3 V

with picamera.PiCamera() as camera:
    camera.start_preview()
    GPIO.wait_for_edge(17, GPIO.FALLING)
    GPIO.output(22, True)
    GPIO.output(23, False)
    camera.capture('/home/pi/Desktop/image1.jpg', use_video_port=True)
    camera.stop_preview
    GPIO.cleanup()
```

- *Annex 2. Training process for Convolutional Neural Network*

```python
import sys
import os
import numpy as np
from tensorflow.python.keras.preprocessing.image import ImageDataGenerator
from tensorflow.python.keras import optimizers
from tensorflow.python.keras.models import Sequential
from tensorflow.python.keras.layers import Dropout, Flatten, Dense,
Activation
from tensorflow.python.keras.layers import Convolution2D, MaxPooling2D
from keras.utils.np_utils import to_categorical
from tensorflow.python.keras import backend as K
from tensorflow.compat.v1 import ConfigProto
from tensorflow.compat.v1 import InteractiveSession

K.clear_session()

data_entrenamiento='./data/entrenamiento'
data_validacion='./data/validacion'
data_test='./data/test'
```

```
### Parameters
epocas = 20
longitud, altura = 300, 300
batch_size = 32
pasos = 500
validation_steps = 5
filtrosConv1 = 32
filtrosConv2 = 64
filtrosConv3 = 128
tamano_filtro1 = (3, 3)
tamano_filtro2 = (3, 3)
tamano_filtro3 = (3, 3)
tamano_pool = (2, 2)
clases = 2              # sintomas, nosintomas
lr = 0.0001

## Preprocesamiento
##Preparamos nuestras imagenes
entrenamiento_datagen = ImageDataGenerator(
    rescale=1. / 255,
    shear_range=0.3,
    zoom_range=0.3,
    horizontal_flip=True
)
validacion_datagen = ImageDataGenerator(
    rescale=1./255
)
test_datagen = ImageDataGenerator(
    rescale=1./255
)
entrenamiento_generator = entrenamiento_datagen.flow_from_directory(
    data_entrenamiento,
    target_size=(altura, longitud),
    batch_size=batch_size,
    class_mode='categorical'
)
validacion_generator=validacion_datagen.flow_from_directory(
    data_validacion,
    target_size=(altura, longitud),
    batch_size=batch_size,
    class_mode='categorical'
)
test_generator = test_datagen.flow_from_directory(
    data_test,
    target_size=(longitud, altura),
    batch_size=batch_size,
    class_mode='categorical')

### Crear la red CNN
cnn = Sequential()
cnn.add(Convolution2D(filtrosConv1, tamano_filtro1, padding='same',
input_shape=(altura, longitud, 3), activation='relu'))
cnn.add(MaxPooling2D(pool_size=tamano_pool))
cnn.add(Convolution2D(filtrosConv2, tamano_filtro2, padding='same',
activation='relu'))
cnn.add(MaxPooling2D(pool_size=tamano_pool))
```

```
cnn.add(Convolution2D(filtrosConv3, tamano_filtro3, padding='same',
activation='relu'))
cnn.add(MaxPooling2D(pool_size=tamano_pool))

cnn.add(Flatten())
cnn.add(Dense(256, activation='relu'))
cnn.add(Dropout(0.5))
cnn.add(Dense(clases, activation='softmax'))

cnn.compile(loss='categorical_crossentropy',
optimizer=optimizers.Adam(lr=lr), metrics=['accuracy'])
cnn.fit_generator(entrenamiento_generator, steps_per_epoch=pasos,
epochs=epocas, validation_data=validacion_generator,
validation_steps=validation_steps)

dir = './modelo/'
if not os.path.exists(dir):
  os.mkdir(dir)
cnn.save('./modelo/modelo.h5')
cnn.save_weights('./modelo/pesos.h5')

cnn.summary()

test_loss,test_acc=cnn.evaluate_generator(test_generator)
print("Test Accuracy:",test_acc)
print("Test Loss:",test_loss)
```

- *Annex 3. Prediction process for Convolutional Neural Network*

```
-  import numpy as np
   from keras.preprocessing.image import load_img, img_to_array
   from keras.models import load_model
   import tensorflow as tf
   longitud, altura=300, 300
   modelo='./modelo/modelo.h5'
   pesos='./modelo/pesos.h5'
   cnn = tf.keras.models.load_model(modelo)
   #cnn = load_model(modelo)
   cnn.load_weights(pesos)

   def predict(file):
     x=load_img(file, target_size=(longitud, altura))
     x=img_to_array(x)
     x=np.expand_dims(x, axis=0)
     arreglo=cnn.predict(x)
     resultado=arreglo[0]
     respuesta=np.argmax(resultado)
     if respuesta == 0:
       print("Pred: Normal Retina")
     elif respuesta == 1:
       print("Pred: Possible Symptoms of Diabetic Retinopathy Detected")
     return respuesta

   predict()
```